

**Block Copolymer-Templated Iron Oxide Nanoparticles for Bimodal Growth of  
Multi-walled Carbon Nanotubes**

By

KYLE E YAZZIE

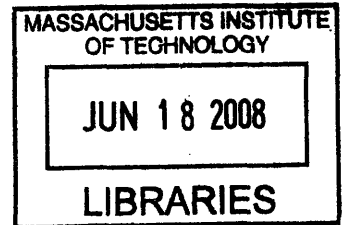
Submitted to the Department of Materials Science and Engineering in Partial Fulfillment  
of the Requirements for the Degree of

Bachelor of Science

at the

Massachusetts Institute of Technology

June 2008



© 2008 Kyle E Yazzie  
All rights reserved

**ARCHIVES**

The author hereby grants to MIT permission to reproduce and to distribute publicly paper  
and electronic copies of this thesis document in whole or in part in any medium now  
known or hereafter created.

Signature of Author.....  
Department of Materials Science and Engineering V V  
May 16, 2008

Certified by.....  
Robert E. Cohen, Ph.D.  
St. Laurent Professor of Chemical Engineering, MIT  
Thesis Advisor

Accepted by.....  
Caroline A. Ross  
Chair, Undergraduate Committee

# **Block Copolymer-Templated Iron Oxide Nanoparticles for Bimodal Growth of Multi-walled Carbon Nanotubes**

by

KYLE E YAZZIE

Submitted to the Department of Materials Science and Engineering in Partial Fulfillment of the Requirements for the Degree of Bachelor of Science at the Massachusetts Institute of Technology

## ***Abstract***

Since their discovery carbon nanotubes (CNTs) have sparked great interest due to their exceptional mechanical, electrical, and thermal properties.<sup>1</sup> These properties make carbon nanotubes desirable for numerous applications including: nanoelectronics, high-strength composites, energy storage, superhydrophobic surfaces, sensors, and biomaterial interfaces.<sup>2,3</sup> Bulk synthesis of carbon nanotubes with controlled physical features, i.e. length, diameter, multiwalled vs. single walled, carbon nanotube chirality, etc. is necessary to make full use of carbon nanotubes' exceptional properties in commercial aspects.

Typical carbon nanotube synthesis processes use chemical vapor deposition (CVD), arc-discharge, and laser ablation.<sup>1</sup> Synthesizing carbon nanotubes via CVD typically involves depositing a thin metal film on a silicon substrate, and heating the substrate so that the thin metal film dewets and forms metallic nanoparticles. A hydrocarbon gas is then flowed over the nanoparticles to initiate carbon nanotube growth.<sup>4</sup> Though these thin metal film catalysts are easy to prepare, they offer poor control over nanoparticle diameters and areal density.<sup>4</sup> It has been shown that physical

properties of carbon nanotubes, such as diameter and uniformity of growth, are directly related to the diameter of the catalyst nanoparticle, and that chirality of the carbon nanotube is inversely related to the catalyst nanoparticle diameter.<sup>2,3,4</sup> Therefore, fully exploiting the unique properties of carbon nanotubes requires an understanding of how to control catalyst nanoparticle diameters, and thereby carbon nanotube physical characteristics. Bennett et al demonstrated that controllability of nanoparticle diameters is possible using a simple poly(styrene-*b*-acrylic acid) (PS-*b*-PAA) amphiphilic block copolymer.<sup>4</sup> The amphiphilic PS-*b*-PAA block copolymer forms micelles, when dissolved in toluene, with anionic carboxylic acid groups available from the PAA. The anionic PAA carboxylic acid groups can be used to sequester metal cations, so that metal is effectively loaded into the micelles. The size of nanoparticles can be controlled by the size of the PAA portion of the block copolymer.<sup>5</sup> When spin cast onto a substrate, the metal-loaded PS-*b*-PAA micelles form a quasi-ordered block copolymer thin film. Maximizing the amount of metal-loaded micelles in solution can maximize the resulting areal density of nanoparticles, thereby forming a monodisperse, quasi-hexagonal nanoparticle array.<sup>5</sup> The deposited micellular thin film and substrate can then be etched with oxygen plasma, removing the organic polymer so that only the nanoparticle array is left, and the substrate is ready for carbon nanotube growth.

Thesis Supervisor: Robert E. Cohen, St. Laurent Professor of Chemical Engineering

## **Acknowledgements**

I would like to extend my most sincere gratitude to Eric Verploegen and the many colleagues that he has introduced me to. His breadth and depth of scientific knowledge and unmitigated enthusiasm has made this thesis project truly educational and fulfilling. I feel incredibly fortunate to have worked with him on this project. Work performed by A. J. Hart and his team of graduate students from the University of Michigan, including Sang Han and Eric Meshot, has contributed substantial matter to this thesis. I would also like to thank Andy Miller for plasma etching several samples, and Teijia Zang for characterizing the nanoparticle arrays with AFM. My thesis advisor, Professor Robert E. Cohen, has my deepest respect and gratitude. His convivial nature and astute intellect has made the process of constructing this thesis rewarding and educational. Finally, I would like to thank my family, who have always supported me, and without whom none of my accomplishments would be possible.

## Table of Contents

LIST OF FIGURES.....	6
LIST OF TABLES.....	11
1 Introduction.....	12
2 Experimental Details.....	17
2.1 Materials.....	17
2.2 Sample Preparation.....	18
2.3 Transmission Electron Microscopy.....	20
2.4 Small-Angle X-ray Scattering and Grazing Incidence Small-Angle X-ray Scattering.....	21
2.5 Growth of Carbon Nanotubes from Nanoparticle Arrays.....	23
2.6 Statistical Analysis of Nanoparticle Diameter Distributions.....	24
3 Results and Discussion.....	26
3.1 Significantly Different Mean Particle Diameters.....	26
3.2 Single PS-b-PAA Block Copolymer and Metal Loading Systems.....	29
3.2.1 Small.....	29
3.2.2 Medium.....	30
3.2.3 Large.....	32
3.3 Summary of nanoparticle diameters available using single systems of one PS-b-PAA block copolymer and one metal loading.....	34
3.4 Combinations of Two Block Copolymer and Metal Loading Systems.....	34
3.4.1 Small + Medium.....	36
3.4.2 Small + Large.....	39
3.4.3 Small + XLarge.....	42
3.5 Additive Relationship between single and combined systems.....	45
3.5.1 Small, Medium, and Small + Medium.....	45
3.5.2 Small, Large, and Small + Large.....	47
3.5.3 Small, and Small + XLarge.....	48
3.6 Summary of nanoparticle diameters available using additive system of nanoparticle arrays.....	50
3.7 Factors affecting the nanoparticle diameter distributions.....	51
3.8 Grazing Incidence Small-angle X-ray Scattering (GISAXS) of Nanoparticle Arrays.....	53
3.9 Small-Angle X-ray Scattering of Carbon Nanotubes Grown From Nanoparticle Arrays.....	56
4 Summary and Conclusions.....	60
5 References.....	63
Appendix A.....	67
Appendix B.....	68
Appendix C.....	73

## List of Figures

- Figure 1 The arrangement of repeat units in a block copolymer, where A and B are chemically dissimilar repeat units.....12
- Figure 2 Chemical formula for poly(styrene-block-acrylic acid). n and m are the number of repeat units constituting each block. The COOH group of the acrylic acid portion of the block copolymer ionizes in solution, and constitutes the anionic core of the micelles.....12
- Figure 3 Microstructure of a micelle formed with block copolymers. Solutions of such micelles, with anionic cores were loaded with  $\text{Fe}^{3+}$  via a reduction of  $\text{FeCl}_3$  salt in solution. This mechanism was used to synthesize the  $\text{Fe}_2\text{O}_3$  nanoparticles studied herein.....12
- Figure 4 Strategies for synthesizing bimodal nanoparticles, using PS-*b*-PAA block copolymer micelles. In Strategy A a single block copolymer with two different metal loadings was used. In Strategy B in two block copolymers with dissimilar molecular weights, containing one metal loading was used. In Strategy C two block copolymers with dissimilar molecular weights, containing two different metal loadings was utilized. Strategy C potentially yields the largest size discrepancy between nanoparticles.....16
- Figure 5 Typical setup for SAXS of carbon nanotube tubes. A motorized stage allows for progressive vertical scans to be taken in the y-direction, at a height h from the substrate surface. (used with permission, Verploegen 2008).....22
- Figure 6 A schematic of a typical GISAXS experiment for a thin film. A collimated X-ray beam is grazed off the sample at an angle,  $\alpha$ . Scattering in the  $q_y$  direction results from features in the plane of the sample surface. Scattering in the  $q_x$  direction results from features parallel to the sample surface. (used with permission, Verploegen 2008).....23
- Figure 7 The left portion of the figure shows the distribution of nanoparticle diameters, and box-and-whisker plots indicating their mean values and range. The particle counts are; 49 for Small, 187 for Medium, and 151 for Large. The right portion of the figure shows the Tukey-Kramer Honestly Significant Difference (HSD) test of the mean nanoparticle diameters. The diameters of the circles represent the nanoparticle diameters that fall within the 95% confidence levels. Circles that intersect at less than or equal to 90° are considered to represent diameters with significantly different means. The Tukey-Kramer HSD shows that the Small, Medium, and Large nanoparticle have significantly different mean diameters. However, the Small and Medium nanoparticles have only borderline significantly different mean diameters. This is not surprising considering that the Small and Medium nanoparticles are synthesized using the same block copolymer, PS<sub>11000</sub>-*b*-PAA<sub>1200</sub>, only with different metal loadings.....26

Figure 8 Distribution of particle diameters for Small ( $PS_{11000}$ - $b$ - $PAA_{1200}$  Metal Loading = 0.5). The total particle count is 49. The normal-quantile plot above the nanoparticle diameter distribution indicates that the diameters are normally distributed. A normal distribution curve was fitted to the Small nanoparticle distribution to give a mean nanoparticle diameter of 5.8 nm with a standard deviation of 1.2 nm. The inset is a representative TEM image of the Small nanoparticle array. The dark blotches, such as the one circled with the dashed line, appear in several TEM images. They did not significantly affect the morphology of the nanoparticles or the particle diameter analysis. The blotches were determined to be due to debris from undissolved polymer in solution or debris ejected onto the backside of the TEM window during the spin casting process.....30

Figure 9 Distribution of particle diameters for Medium ( $PS_{11000}$ - $b$ - $PAA_{1200}$  Metal Loading = 5). The total particle count is 187 particles. The normal-quantile plot above the nanoparticle diameter distribution indicates that the diameters are normally distributed. A normal distribution curve was fitted to the Medium nanoparticle distribution to give a mean nanoparticle diameter of 6.8 nm with a standard deviation of 2.2 nm. The inset is a representative TEM image of the Medium nanoparticle array.....31

Figure 10 Distribution of particle diameters for Large ( $PS_{16500}$ - $b$ - $PAA_{4500}$  Metal Loading = 5). The total particle count is 150. The normal-quantile plot above the nanoparticle diameter distribution indicates that the diameters are normally distributed. A normal distribution curve was fitted to the Large nanoparticle distributions to give a mean nanoparticle diameter of 12.07 nm with a standard deviation of 2.70 nm. The inset is a representative TEM image of the Large nanoparticle array. The hollow appearance of the nanoparticles was determined to be caused by focusing effects in the TEM, and do not reflect a true morphological characteristic of the nanoparticles. Similar conclusions about nanoparticles that appear hollow were reached by Bennett 2007. The spread of the nanoparticle diameter distribution can be attributed to the irregularly shaped Large nanoparticles, as seen in the inset TEM image.....33

Figure 11 Distribution of particle diameters for a combined solution of Small and Medium solutions ( $PS_{11000}$ - $b$ - $PAA_{1200}$  Metal Loading = 0.5 +  $PS_{11000}$ - $b$ - $PAA_{1200}$  Metal Loading = 5). The normal-quantile plot above the nanoparticle diameter distribution indicates that the diameters are not normally distributed. The inset is a representative TEM image of the Small + Medium nanoparticle array.....37

Figure 12 The unimodal nanoparticle diameter distributions that constitute the non-normal Small + Medium nanoparticle diameter distribution are shown extracted to the right. The unimodal nanoparticle diameter distributions are normally distributed with means and standard deviations of 5.19 nm  $\pm$  0.89 nm for the top distribution and 9.8 nm  $\pm$  1.06 nm for the bottom distribution. The unimodal nanoparticle diameter distributions represent the Small and Medium constituents of the Small + Medium nanoparticle diameter distribution because the standard deviations for the Small distributions overlap and the standard deviations for the Medium distributions overlap.....38

Figure 13 Distribution of particle diameters for a combined solution of Small and Large solutions (PS<sub>11000</sub>-*b*-PAA<sub>1200</sub> Metal Loading = 0.5 + PS<sub>16500</sub>-*b*-PAA<sub>4500</sub> Metal Loading = 5). The total particle count is 97 particles. The normal-quantile plot above the nanoparticle diameter distribution indicates that the diameters are not normally distributed. The inset is a representative TEM image of the Small + Large nanoparticle array.....40

Figure 14 The unimodal nanoparticle diameter distributions that constitute the non-normal Small + Large nanoparticle diameter distribution are shown extracted to the right. The unimodal nanoparticle diameter distributions are normally distributed with means and standard deviations of 5.55 nm ± 1.40 nm for the top distribution and 11.70 nm ± 1.80 nm for the bottom distribution. The unimodal nanoparticle diameter distributions represent the Small and Large constituents of the Small + Large nanoparticle diameter distribution because the standard deviations for the Small distributions overlap and the standard deviations for the Large distributions overlap.....41

Figure 15 Distribution of particle diameters for a combined solution of Small and XLarge solutions (PS<sub>11000</sub>-*b*-PAA<sub>1200</sub> Metal Loading = 0.5 + PS<sub>2200</sub>-*b*-PAA<sub>11500</sub> Metal Loading = 5). The total particle count is 137 particles. The normal-quantile plot above the nanoparticle diameter distribution indicates that the diameters are not normally distributed. The inset is a representative TEM image of the Small + XLarge nanoparticle array.....43

Figure 16 The unimodal nanoparticle diameter distributions that constitute the non-normal Small + XLarge nanoparticle diameter distribution are shown, extracted to the right. The unimodal nanoparticle diameter distributions are normally distributed with means and standard deviations of 5.55 nm ± 1.40 nm for the top distribution and 12.47 nm ± 1.46 nm for the bottom distribution. The unimodal nanoparticle diameter distributions represent the Small and XLarge constituents of the Small + XLarge nanoparticle diameter distribution.....44

Figure 17 A superposition of the single Small and Medium diameter distributions, and the Small + Medium diameter distribution is shown. The diameter distribution for the Small nanoparticles is indicated in gray, and has a mean diameter of 5.8 nm with a standard deviation of 1.2 nm. The diameter distribution for the Medium nanoparticles is indicated in black, and has a mean diameter of 6.8 nm with a standard deviation of 2.2 nm. The diameter distribution for the combined Small + Medium nanoparticles is indicated in diagonal black lines. The decomposed unimodal distributions of Small + Medium have a low mean of 5.19 nm with a standard deviation of 0.89 nm, and a high mean of 9.8 nm with a standard deviation of 1.06 nm. The low and high unimodal means correspond to the means of the single Small and Medium diameter distributions, with standard deviations that overlap.....46

Figure 18 A superposition of the single Small and Large diameter distributions, and the Small + Large diameter distribution is shown. The diameter distribution for the Small



nanoparticles is indicated in gray, and has a mean diameter of 5.80 nm with a standard deviation of 1.20 nm. The diameter distribution for the Large nanoparticles is indicated in black, and has a mean diameter of 12.09 nm with a standard deviation of 2.70 nm. The diameter distribution for the combined Small + Large nanoparticles is indicated in diagonal black lines. The decomposed unimodal distributions of Small + Large have a low mean of 5.50 nm with a standard deviation of 1.40 nm, and a high mean of 11.70 nm with a standard deviation of 1.80 nm. The low and high unimodal means correspond to the means of the single Small and Large diameter distributions, with standard deviations that overlap.....48

Figure 19 An overlay of the single solution Small, and the combined solution Small + XLarge histograms is shown. The diameter distribution for the Small nanoparticles is indicated in gray and has a mean diameter of 5.80 nm with a standard deviation of 1.20 nm. The diameter distribution for the combined Small + XLarge nanoparticles is indicated in diagonal black lines. The decomposed unimodal distributions of Small + XLarge have a low mean of 5.51 nm with a standard deviation of 1.50 nm, and a high mean of 12.47 nm with a standard deviation of 1.46 nm. The low and high unimodal means correspond to the means of the single Small and XLarge diameter distributions, with standard deviations that overlap for the Small diameter nanoparticles.....50

Figure 20 A representative grazing incidence small-angle X-ray scattering (GISAXS) image taken of nanoparticle array. Structure factor scattering related to spacing between the nanoparticles is indicated with a black arrow.....54

Figure 21 GISAXS intensities for a Large nanoparticle array that is heated from room temperature (30 °C) to the typical carbon nanotube growth temperature (820 °C) are shown. This process is termed annealing. Annealing is performed routinely on metallic nanoparticle arrays used for catalyzing carbon nanotube growth. The structure factor peak is indicated with a black arrow. It can be seen that the intensity of the structure factor peak disappears as the Large nanoparticle array is annealed. This indicates a slight rearrangement of the nanoparticles.....55

Figure 22 A small-angle X-ray scattering (SAXS) image of a carbon nanotube forest grown from a Large diameter nanoparticle array. The SAXS image indicates vertical alignment for the carbon nanotube forest.....56

Figure 23 SAXS intensities for a carbon nanotube forest grown from an array of Large diameter nanoparticles. For this analysis  $c = 0.5$ , the average diameter was 6.9 nm, the standard deviation was 0.82 nm, and the Hermans orientation factor was 0.52.....57

Figure 24 TEM image of carbon nanotubes grown from a Large diameter nanoparticle array. SAXS analysis indicated that the carbon nanotubes grown from the Large diameter nanoparticle arrays had an average diameter of 6.9 nm with a standard deviation of 0.82 nm. The Hermans orientation factor was 0.52. The carbon nanotubes are supported on a holey carbon film.....58

Figure 25 SAXS intensities for a carbon nanotube forest grown from an array of XLarge diameter nanoparticles. For this analysis  $c = 0.7$ , the average diameter was 6.4 nm, the standard deviation was 1.2 nm, and the Hermans orientation factor was close to 0.....58

Figure 26 A defect in the walls of a multi-walled carbon nanotube.....67

Figure 27 GISAXS intensity plot for the Medium 0.5 wt% (black curve) and Medium 0.2 wt% (gray curve) nanoparticle arrays. The Medium 0.5 wt% solution used to fabricate the nanoparticle array had equilibrated for 6 months prior to the sample being spin cast. The Medium 0.2 wt% solution used to fabricate the nanoparticle array had equilibrated for 7 months prior to the sample being spin cast. The inter-particle for the Medium 0.5 wt% 6 month and Medium 0.2 wt% 7 month nanoparticle arrays are 20 nm and 17 nm, respectively.....69

Figure 28 GISAXS intensity plot for the Large 0.5 wt% (black curve) and Large 0.2 wt% (gray curve) nanoparticle arrays. The Large 0.5 wt% solution used to fabricate the nanoparticle array had equilibrated for 6 months prior to the sample being spin cast. The Large 0.2 wt% solution used to fabricate the nanoparticle array had equilibrated for 7 months prior to the sample being spin cast. The inter-particle for the Large 0.5 wt% 6 month and Large 0.2 wt% 7 month nanoparticle arrays are 28 nm and 27 nm, respectively.....70

Figure 29 GISAXS intensity plot for the Small + Large 0.5 wt% (black curve) and Small + Large 0.2 wt% (gray curve) nanoparticle arrays. The Small + Large 0.5 wt% solution used to fabricate the nanoparticle array had equilibrated for 6 months prior to the sample being spin cast. The Small + Large 0.2 wt% solution used to fabricate the nanoparticle array had equilibrated for 7 months prior to the sample being spin cast. The inter-particle for the Small + Large 0.5 wt% 6 month and Small + Large 0.2 wt% 7 month nanoparticle arrays are 28 nm and 26 nm, respectively.....71

## List of Tables

Table 1 The poly(styrene-*block*-acrylic acid) copolymers used and their respective block lengths are listed below. The molecular weights of each block are denoted in subscript, in units of g/mol. The metal loadings that were used with each block copolymer in solution are also listed. Metal loading is the metal ion equivalents per carboxylic acid group. Relative size refers to the expected size of each micelle, relative to one another.....18

Table 2 A summary of the mean nanoparticle diameters available, and the standard deviations for the Small, Medium, and Large PS-*b*-PAA block copolymer and metal loading systems is shown below. No data was available for XLarge at the time that this report was written. The XLarge category is included for completeness.....34

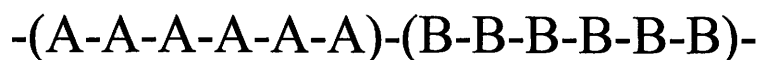
Table 3 The peak nanoparticle diameters available for a combined set of block copolymers and metal loadings are indicated in the table.....51

Table 4 Listed below are the nanoparticle arrays for which there were adequate data to plot intensities. The plotted intensities yielded intensity peaks, due to the structure factor of the nanoparticles, that made it possible to calculate the inter-particle spacing. The solution concentration, equilibrium time, and inter-particle spacing are listed.....72

Table 5 The diameters of carbon nanotubes grown from nanoparticle arrays that were spin cast from 0.5 wt% solutions are shown. Only the XLarge and XLarge + Small nanoparticle arrays that grew carbon nanotubes are listed. These carbon nanotube forests produced enough SAXS intensity to be analyzed.....74

## 1. Introduction

Copolymers are polymers that have more than one chemically dissimilar repeat unit in their molecular chain.<sup>6</sup> The arrangement of the dissimilar repeat units may be block, random, alternating, or graft. The block, random, and alternating arrangement of copolymer repeat units produce linear polymer chains. In block copolymers the copolymer repeat units are arranged in continuous sections of one type of repeat unit, as illustrated in Figure 1.



**Figure 1** The arrangement of repeat units in a block copolymer, where A and B are chemically dissimilar repeat units.

In this study, the diblock copolymer used was poly(styrene-*block*-acrylic acid) PS-*b*-PAA.

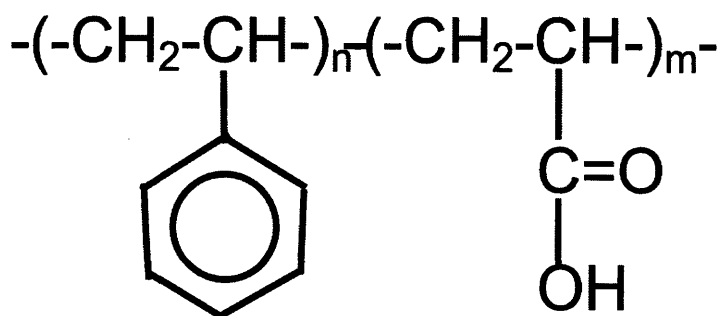


**Figure 2** Chemical formula for poly(styrene-*block*-acrylic acid). n and m are the number of repeat units constituting each block. The COOH group of the acrylic acid portion of the block copolymer ionizes in solution, and constitutes the anionic core of the micelles.

The dissimilar block sections of a copolymer produce a range of morphologically distinct phases if the blocks are immiscible with the surrounding medium. Increasing the asymmetry of the diblock copolymer sections can result in lamellar, rod, and spherical morphologies.<sup>7</sup> Spherical morphologies of diblock copolymers are termed micelles.

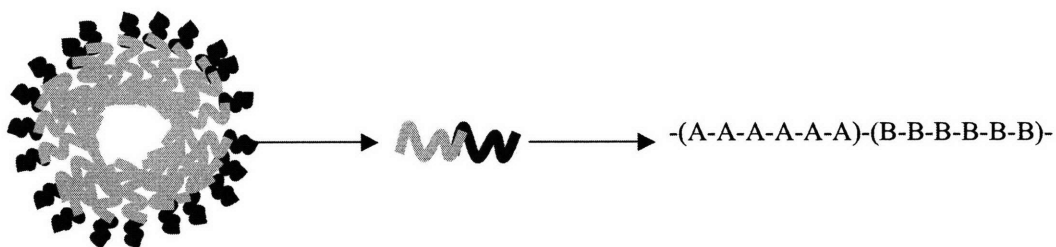


**Figure 3 Microstructure of a micelle formed with block copolymers. Solutions of such micelles, with anionic cores were loaded with  $\text{Fe}^{3+}$  via a reduction of  $\text{FeCl}_3$  salt in solution. This mechanism was used to synthesize the  $\text{Fe}_2\text{O}_3$  nanoparticles studied herein.**

The arrangements of diblock copolymer micelles in solution are such that block sections, that are soluble in the solution, make up the surface, or corona, of the micelle. The interior of the micelle is composed of the diblock section that is insoluble in the solution.<sup>7,8</sup> For this report PS-*b*-PAA was dissolved in toluene. The PS polymer unit is soluble in toluene and forms the corona of the PS-*b*-PAA micelle. The self-assembly of diblock copolymers into micelles makes them ideal structures for sequestering inorganic or organic species and keeping those species separate from the surrounding medium. The carboxylic acid groups in PS-*b*-PAA become anionic in solution, losing  $\text{H}^+$  ions. When ionized in solution, the acrylic acid groups make excellent reducers for metallic species. When PS-*b*-PAA is in the micelle phase, the micelles serve as nanoreactors.<sup>9</sup> The internal environment of micelles is often purer than bulk processing environments.

PS-*b*-PAA may be used to synthesize inorganic nanoparticles from precursor metallic salts.<sup>9,10</sup> In several cases this mechanism of synthesizing inorganic nanoparticles is used to create metal-polymer nanocomposites. In those studies no particular attention was paid to controlling the diameters of the metallic nanoparticles that were synthesized. Recent work done by Bennett et al. 2006 has elaborated on the metal-loaded micelle technique for creating inorganic nanoparticles, by introducing block copolymers with varying block lengths of PAA. Varying the block length of the PAA, and varying the amount of metal species that was put into solution with the micelles was shown to provide an elegant means of controlling the diameters of metallic nanoparticles synthesized via that technique.<sup>4,5</sup>

Inorganic nanoparticles can be used as catalysts for synthesizing carbon nanotubes.<sup>4,5,11</sup> A hydrocarbon gas, such as ethylene, is flowed over inorganic nanoparticles that are supported on a heated substrate. The hydrocarbon gas decomposes on the surfaces of the inorganic nanoparticles and begins to catalyze carbon nanotube growth. The specific mechanism by which carbon nanotubes grow on the surface of the inorganic nanoparticles is not fully understood at present. It has been proposed that the size of the inorganic nanoparticle catalyst can control the number of walls that the carbon nanotube has, and its chirality.<sup>2,3,4</sup> Controlling the morphology and chirality of carbon nanotubes becomes necessary when specific applications are addressed, e.g. composite reinforcement, electronic components, biomaterials, etc.

The technique developed by Bennett et al. 2006 has been shown to yield inorganic nanoparticles with diameters that are tunable using PS-*b*-PAA block copolymers with varying molecular weights and metal loadings. Bennett et al. showed that this technique

could be used to synthesize a normally distributed, narrow range of carbon nanotube diameters from a monodisperse array of inorganic nanoparticles. This technique is also useful for varying the areal density of nanoparticle arrays. Varying the areal density directly affects the morphology of the carbon nanotube forests grown from the inorganic nanoparticle arrays.

In this study, the concept of using tunable micelles to synthesize inorganic nanoparticle arrays for catalyzing carbon nanotube growth is extended to the synthesis of bimodal nanoparticle arrays. Several types of PS-*b*-PAA block copolymer with varying block lengths were put into solution with toluene to create micelles with different domain sizes. The relative amounts of metal species that were loaded into the micelles were also varied. Varying both the size of the PAA core of the micelles and their metal loading would provide several options for creating nanoparticles of dissimilar sizes. The combinations of PS-*b*-PAA block copolymer and metal loadings resulted in three strategies to obtain a bimodal distribution of nanoparticle diameters. In the first strategy, referred to as Strategy A in Figure 4, a single type of block copolymer with two different metal loadings was used. In the second strategy, referred to as Strategy B in Figure 4, two types of block copolymers with dissimilar molecular weights, containing one metal loading, was used. In the third strategy, referred to as Strategy C in Figure 4, two types of block copolymers with dissimilar molecular weights, containing two different metal loadings was utilized. Strategy A potentially yields the smallest size discrepancy between nanoparticles. Strategy C potentially yields the largest size discrepancy. Strategy B was not analyzed in this study, because Strategies A and C were thought to provide

greater insight into the maximum and minimum discrepancy possible using the metal loaded PS-*b*-PAA block copolymer micelle systems.

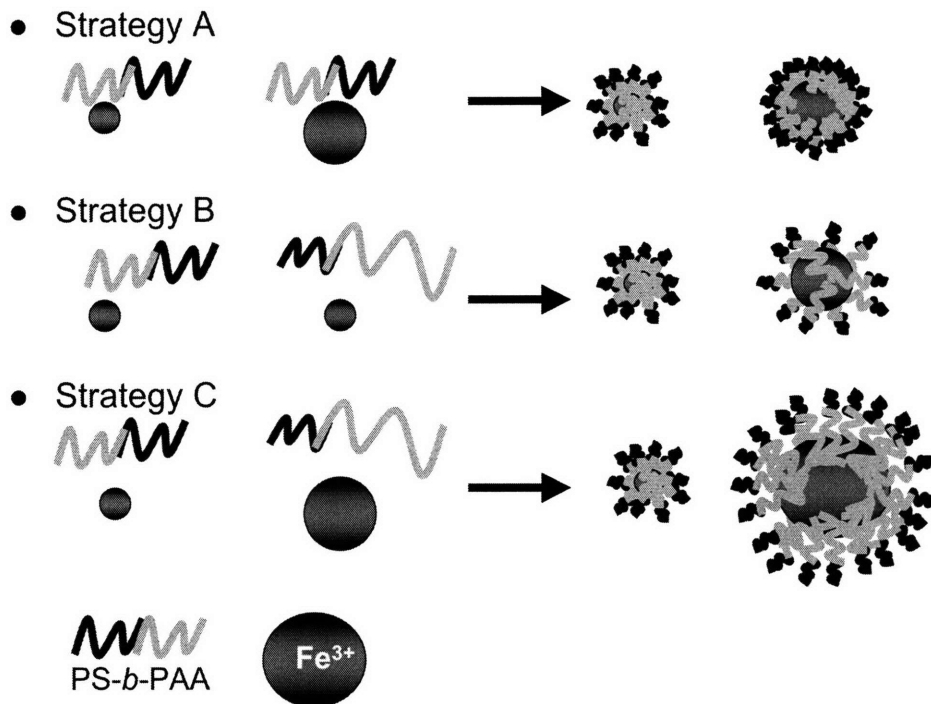


**Figure 4 Strategies for synthesizing bimodal nanoparticles, using PS-*b*-PAA block copolymer micelles. In Strategy A a single block copolymer with two different metal loadings was used. In Strategy B in two block copolymers with dissimilar molecular weights, containing one metal loading was used. In Strategy C two block copolymers with dissimilar molecular weights, containing two different metal loadings was utilized. Strategy C potentially yields the largest size discrepancy between nanoparticles.**

Nanoparticle arrays fabricated in this study were characterized using transmission electron microscopy (TEM) and small-angle X-ray scattering (SAXS) techniques. Techniques such as small-angle X-ray scattering (SAXS), and grazing incidence small-angle X-ray scattering (GISAXS) are powerful tools used to gain insight into the morphology of a large number of discrete features; as is the case with carbon nanotube



forests and nanoparticle arrays. In SAXS a high-energy ( $\sim 10$ 's –  $100$ 's of eV) collimated X-ray beam is aimed at a sample. Elastic bombardment of the X-rays gives information about the sample. The small-angle scattering ( $1$ - $10^\circ$  typically) provides nanometer scale structural information about the sample.<sup>12</sup> In GISAXS, a high-energy beam of X-rays is aimed at a sample, at a grazing angle  $\alpha$ . Aiming the GISAXS beam in this fashion provides structural information about primarily two-dimensional samples on a surface, e.g. thin forests, nanoparticle arrays, spin cast polymers, etc.<sup>12</sup> In this study SAXS was used to determine the morphology of carbon nanotube forests synthesized from the bimodal nanoparticle arrays. GISAXS was used to determine the morphology and spacing of nanoparticles in arrays.

## **2. Experimental Details**

### **2.1. Materials**

Table 1 shows the PS-*b*-PAA block copolymers that were used to create micelles in solution with toluene, and the molecular weights of each block. The PS-*b*-PAA block copolymers were used as received from Polymer Source, Inc.

**Table 1** The poly(styrene-*block*-acrylic acid) copolymers used and their respective block lengths are listed below. The molecular weights of each block are denoted in subscript, in units of g/mol. The metal loadings that were used with each block copolymer in solution are also listed. Metal loading is the metal ion equivalents per carboxylic acid group. Relative size refers to the expected size of each micelle, relative to one another.

PS- <i>b</i> -PAA Block Copolymers and Metal Loadings			
Relative Sizes	Block Copolymers	Metal Loading	FeCl <sub>3</sub> required (g/mL)
Small	PS <sub>11000</sub> - <i>b</i> -PAA <sub>1200</sub>	0.5	0.00055
Medium	PS <sub>11000</sub> - <i>b</i> -PAA <sub>1200</sub>	5	0.00554
Small	PS <sub>11000</sub> - <i>b</i> -PAA <sub>1200</sub>	0.5	0.00055
Large	PS <sub>16500</sub> - <i>b</i> -PAA <sub>4500</sub>	5	0.01207
Small	PS <sub>11000</sub> - <i>b</i> -PAA <sub>1200</sub>	0.5	0.00055
XLarge	PS <sub>2200</sub> - <i>b</i> -PAA <sub>11500</sub>	5	0.04727

Metal loadings are metal ion equivalents per carboxylic acid group. The metal salt used for metal loading of the poly(styrene-*block*-acrylic acid) micelles was anhydrous iron(III) chloride, FeCl<sub>3</sub>. The anhydrous iron(III) chloride was used as received from Sigma-Aldrich Co. Toluene was obtained from an Innovative Technology Pure-Solv 400 Solvent Purification System.

## 2.2. Sample Preparation

Poly(styrene-*block*-acrylic acid) was measured and put into solution with toluene at a concentration of 0.005 g/mL. Early samples indicated that 0.005 g/mL may have been too concentrated to provide a monolayer of micelles when spin cast. Consequently, a second set of poly(styrene-*block*-acrylic acid) and toluene solutions\* were created with a

\* Previous work had indicated that the poly(styrene-*block*-acrylic acid) solution had to be heated and cooled in order to kinetically lock the block copolymers into the micelle phase.<sup>4</sup> However, in this study it was found that the heat treatment of the solution was not

concentration of 0.002 g/mL. The poly(styrene-*block*-acrylic acid) copolymers with the lower PAA block lengths dissolved easily in the toluene solution. However the poly(styrene-*block*-acrylic acid) copolymer with the largest PAA block length, PS<sub>2200</sub>-*b*-PAA<sub>11500</sub>, did not dissolve easily. In this case, the poly(styrene-*block*-acrylic acid) and toluene solution was sonicated on low power for up to 1 and ½ hours.<sup>†</sup>

The amount of FeCl<sub>3</sub> that is required for a particular concentration of poly(styrene-*block*-acrylic acid) in toluene, and for a particular metal loading is calculated in the following manner; given block copolymer PS<sub>n</sub>-*b*-PAA<sub>m</sub>, where n and m are the respective molar masses of each block length, the metal loading is calculated as:

$$n + m = \text{total molar mass (g/mol)}$$

$$\frac{m \text{ (g/mol)}}{\text{total molar mass (g/mol)}} = \% \text{ PAA}$$

$$\text{“Effective acrylic acid molar mass”} = \frac{\text{acrylic acid molar mass (72 g/mol)}}{\% \text{ PAA}}$$

$$\text{Acrylic acid groups available} = \frac{\text{Solution concentration (0.5 wt\%)}}{\text{“Effective acrylic acid molar mass”}}$$

$$\text{Grams FeCl}_3 \text{ per mL solution} = \text{Acrylic acid groups required} \times \text{molar mass FeCl}_3 \text{ (162 g/mol)}$$

---

necessary to obtain micelles. Further more it was apparent that the heat treatment may have created block copolymer films and debris that contaminated spin cast samples.

<sup>†</sup> Miniscule pieces of undissolved PS<sub>2200</sub>-*b*-PAA<sub>11500</sub> was still visible, even after sonication. Debris in the solutions was allowed to settle before using the solutions for spin casting. Clear solution above the debris layer that settled on the bottom was also transferred to new vials.

**Grams FeCl<sub>3</sub> per mL solution required for metal loading = metal loading (0.5 or 5) x Grams FeCl<sub>3</sub> per mL solution**

Once the proper metal loading is added to the poly(styrene-*block*-acrylic acid) and toluene solution, the solution is gently shaken and allowed to equilibrate for 24 hours. Spin casting was performed at 8000 rpm for 1 minute. For single solution spin casts, the substrate surface is completely covered with metal-loaded poly(styrene-*block*-acrylic acid) micelle solution and the spin speed rapidly increased to 8000 RPM. Combinations of solutions were prepared by combining equal amounts of each solution in a vial and mixing for no longer than 5 seconds, before covering the substrate surface with the combined solutions and spin casting. Allowing the metal loaded PS-*b*-PAA block copolymer micelle solutions to mix longer than 5 seconds was found to result in homogenization of metal loadings within the micelles. This phenomena is discussed further in 3.7. Table 1 lists the combinations of poly(styrene-*block*-acrylic acid) solution and metal loadings that were spin cast to obtain bimodal nanoparticle arrays. Spin cast samples were oxygen plasma etched at 8-12 MHz for 10-15 minutes. Oxygen plasma etching removed the block copolymer thin film and oxidized the Fe<sup>3+</sup> nanoparticles so that an array of Fe<sub>2</sub>O<sub>3</sub> nanoparticles remained on the sample surface.

### **2.3. Transmission Electron Microscopy**

Nanoparticle arrays prepared for transmission electron microscopy (TEM) were spin cast on electron-transparent silicon nitride (Si<sub>3</sub>N<sub>4</sub>) TEM windows. The window

region of the silicon nitride was 100 nm thick. Silicon nitride TEM windows were purchased from SPI Supplies. Carbon nanotube samples were prepared by removing a piece of the carbon nanotube forest from the bulk sample, immersing in isopropyl alcohol, and sonicating on low power for less than 10 seconds to break up the forest. The dispersed carbon nanotubes in isopropyl alcohol was then dropped, with a pipette, onto holey carbon film coated copper grids. Holey carbon film coated copper grids were purchased from SPI Supplies. Transmission electron microscopy was performed on a JEOL 2011 at 200 kV.

#### **2.4. Small-Angle X-ray Scattering and Grazing Incidence Small-Angle X-ray Scattering**

Small-angle X-ray scattering (SAXS) and grazing-incidence small-angle X-ray scattering (GISAXS) experiments were performed at the G1 beamline at the Cornell High Energy Synchrotron Source (CHESS). The wavelength of the X-rays was 1.239Å and silver behenate was used to calibrate the sample to detector distance with a first order scattering vector of  $q$  of  $1.076\text{nm}^{-1}$  (with  $q = 4\pi \sin\theta/\lambda$ , where  $2\theta$  is the scattering angle and  $\lambda$  is the wavelength). A slow-scan CCD-based X-ray detector, home built by Drs. M.W. Tate and S.M. Gruner of the Cornell University Physics Department, was used for data collection. Additional SAXS studies were performed at the X27 beamline at the National Synchrotron Light Source (NSLS) at Brookhaven National Laboratory (BNL), where the wavelength was 0.1371nm. Data was collected with a MarCCD X-ray detector.

SAXS was used to characterize the morphology of carbon nanotube forests grown using the PS-*b*-PAA block copolymer templated nanoparticle arrays. SAXS gave

information about the alignment of the carbon nanotubes and about the modality of their diameter distribution. Figure 5 below shows a schematic of a typical SAXS experiment setup for carbon nanotube forests.

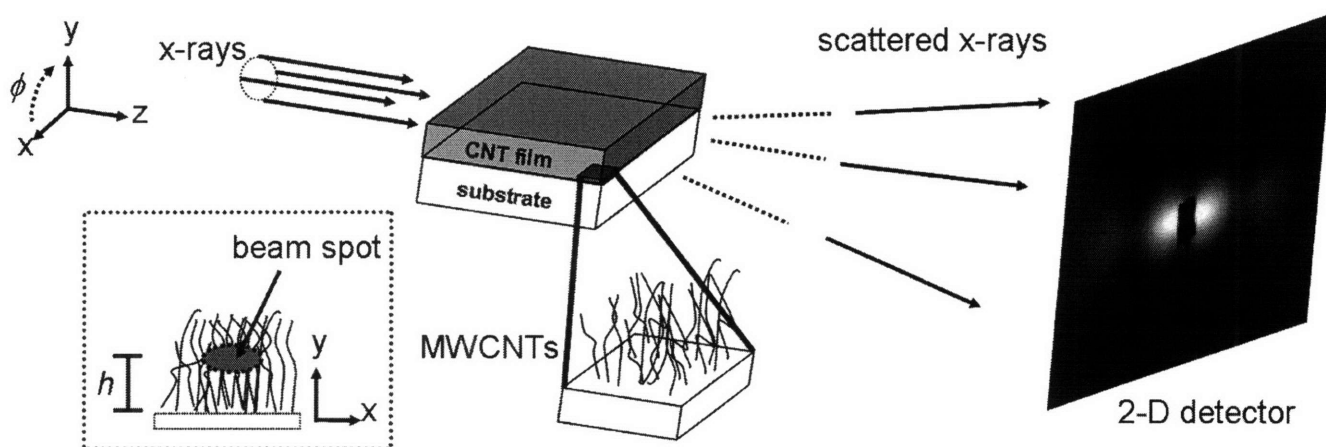


**Figure 5 Typical setup for SAXS of carbon nanotube tubes. A motorized stage allows for progressive vertical scans to be taken in the y-direction, at a height  $h$  from the substrate surface. (used with permission, Verploegen 2008)**

GISAXS was used to characterize the morphology of the  $\text{Fe}_2\text{O}_3$  nanoparticle arrays templated using block copolymer micelles. GISAXS gave information about the inter-particle spacing and about the modality of the nanoparticle diameter distributions. Figure 6 below is a schematic of a typical GISAXS experiment setup for thin films. Thin films were not analyzed in this report, but the extension of GISAXS from thin film analysis to nanoparticle array analysis is trivial.

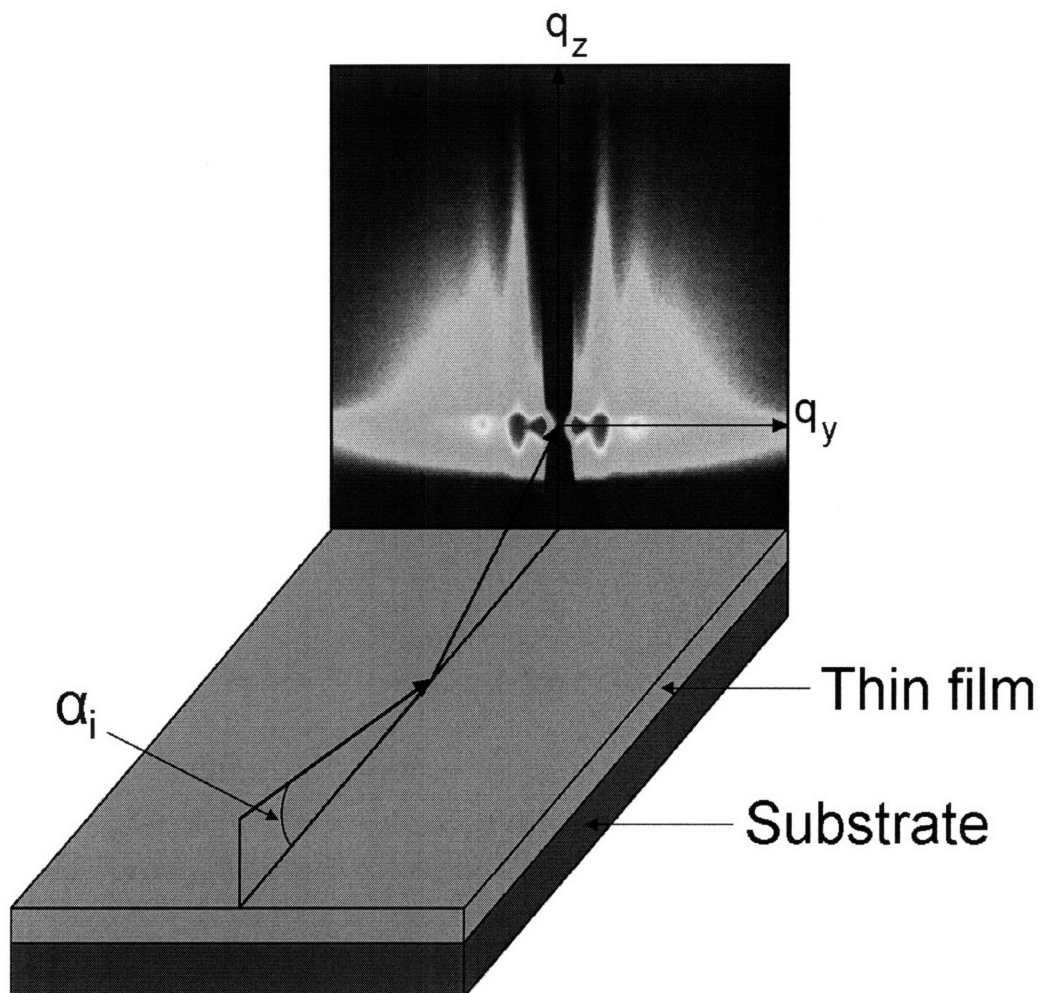


**Figure 6** A schematic of a typical GISAXS experiment for a thin film. A collimated X-ray beam is grazed off the sample at an angle,  $\alpha$ . Scattering in the  $q_y$  direction results from features in the plane of the sample surface. Scattering in the  $q_x$  direction results from features parallel to the sample surface. (used with permission, Verploegen 2008)

## 2.5. Growth of Carbon Nanotubes from Nanoparticle Arrays

Stacking and agglomeration of nanoparticles was found to be a problem for PS-*b*-PAA solutions of 0.5 wt%. Nanoparticle agglomerates are not desirable for carbon nanotube synthesis. The spin cast nanoparticle arrays used to synthesize carbon nanotube growth were from PS-*b*-PAA solutions that were diluted from 0.5 wt% to 0.2 wt%. After the PS-*b*-PAA solutions were diluted from 0.5 wt% to 0.2 wt% no

agglomeration was noticed in TEM. While dilution prevented nanoparticle agglomerates from forming the diluted solutions did not provide nanoparticle arrays with enough areal density to catalyze carbon nanotube growth.<sup>‡</sup> These results are discussed further in 3.9. The samples were placed in a tube furnace that housed a slightly conductive p-doped Si substrate. Current was passed through the p-doped Si substrate so that the surface temperature of the sample placed on top of the substrate could be controlled using resistive heating. The resistive heater and sample are enclosed in a small gas flow chamber. The procedure used to synthesize carbon nanotubes using the nanoparticle arrays was the following:

- He gas was flowed at 400 sccm. The sample is heated from room temperature to 775 °C for 10 minutes.
- He gas flow of 400 sccm is held for 9 minutes at 775 °C.
- He/H<sub>2</sub> gases were flowed at 100/400 sccm, respectively, and held at 775 °C for 1 minute.
- C<sub>2</sub>H<sub>4</sub>/He/H<sub>2</sub> gases were flowed at 100/100/400 sccm, respectively, and held at 775 °C for 15 minutes.

## 2.6. Statistical Analysis of Nanoparticle Diameter Distributions

Statistical analysis of nanoparticle diameter distributions is utilized as a quantitative measurement of the overall distribution of nanoparticle sizes present in a nanoparticle array. Though the concept of using TEM images of particles to obtain a

---

<sup>‡</sup> Recent work using 0.5 wt% metal loaded PS-*b*-PAA block copolymer micelle solutions has yielded nanoparticle arrays with a high enough areal density to catalyze significant carbon nanotube growth.



statistical measurement of the particles is not new, Woehrle et al. 2006 described how this process should be implemented using a public domain image processing software, ImageJ. ImageJ was used to perform particle counts on selected regions of TEM images of the PS-*b*-PAA templated Fe<sub>2</sub>O<sub>3</sub> nanoparticles. Great care was taken to ensure that the selected regions analyzed were representative of the whole sample. Large areas of nanoparticle arrays, on several samples, were surveyed to ensure that the selected image area was representative of that sample set.

To perform the particle count, the TEM image is opened in ImageJ. The TEM image scale bar is used to calibrate the pixel-per-length scale provided by ImageJ. A threshold is taken of a selected region, so that only the nanoparticles visible in the TEM image are highlighted for counting. Thresholding effectively sets a cutoff intensity for the features of the TEM image that will be counted. Particle counting is calibrated using three variables in ImageJ; particle circularity, 'exclude on edges', and 'include holes'. Circularity refers to how circular a particle is. Circularity is quantified by the value,  $\text{circularity} = 4\pi(\text{area}/\text{perimeter}^2)$ , where area and perimeter are for the measured particle. Circularity ranges from 0 to 1, where 0 is an increasingly elongated particle, and 1 is a perfect circle. Intensity inhomogeneities over the surface of the TEM image, and the over the surface of the nanoparticle often causes thresholding to yield particles that have circularity  $\geq 0.25$ . Intensity inhomogeneities can also produce holes in the center of the particles when the threshold is taken. Therefore circularity of 0.25-1 was used. This circularity range was found to reliably exclude erroneous particle counts due to background noise. The 'include holes' and 'exclude on edges' options were chosen to optimize the particle

count. Once a particle count is tallied for the image, the particle diameters are calculated from the particle areas and plotted in a histogram with bin sizes equal to 1 nm. JMP 7 Statistical Discovery software was used to fit normal distribution curves to the single solution nanoparticle arrays, and for the combined solution nanoparticle arrays. Normal-quantile plots were obtained for each normal curve fit.

### **3. Results and Discussion**

#### **3.1. Significantly Different Mean Particle Diameters**

The statistically significant difference between the mean particle diameters for the single systems of one block copolymer and one metal loading was determined using a Tukey-Kramer Honestly Significant Difference (HSD) test, with a p-value of  $> 0.05$ . Tukey-Kramer HSD test for statistically significant difference was chosen because it is a test typically used for data sets of different sizes. Figure 7 below shows the outcome of the Tukey-Kramer HSD test for the nanoparticle arrays synthesized from one block copolymer and one metal loading: Small, Medium, and Large. No data was available for XLarge nanoparticle arrays at the time this report was written.

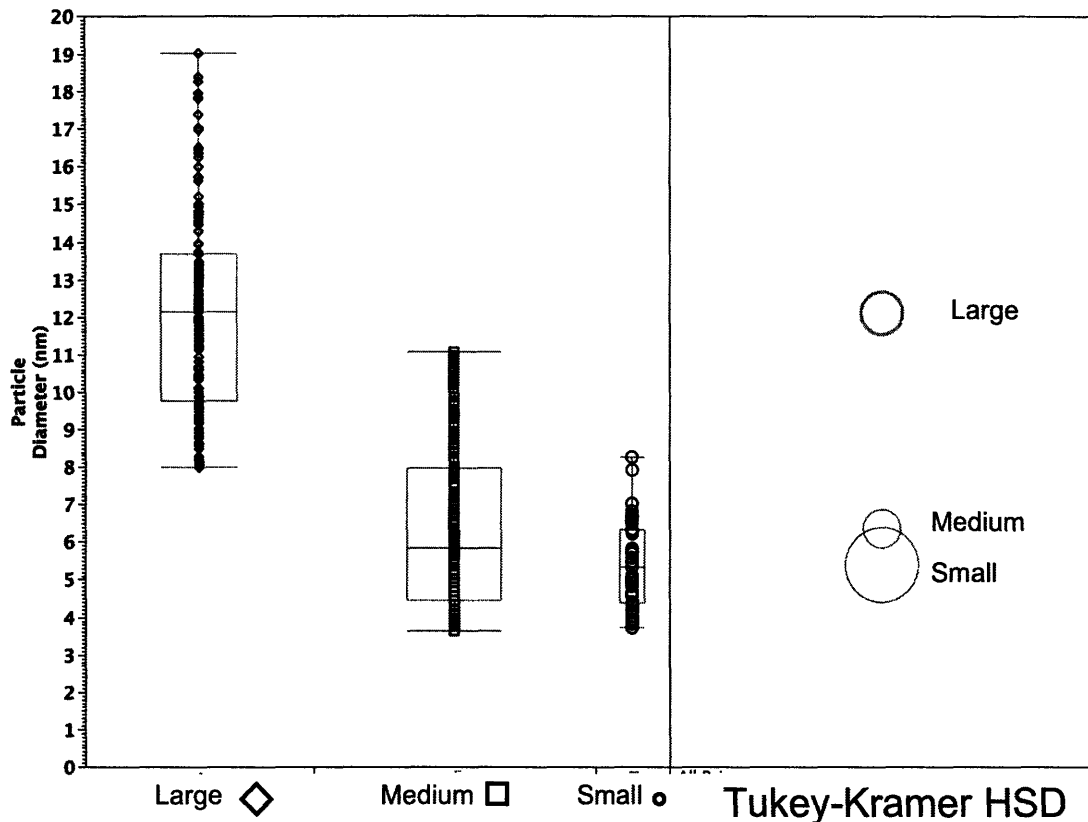


**Figure 7** The left portion of the figure shows the distribution of nanoparticle diameters, and box-and-whisker plots indicating their mean values and range. The particle counts are; 49 for Small, 187 for Medium, and 151 for Large. The right portion of the figure shows the Tukey-Kramer Honestly Significant Difference (HSD) test of the mean nanoparticle diameters. The diameters of the circles represent the nanoparticle diameters that fall within the 95% confidence levels. Circles that intersect at less than or equal to  $90^\circ$  are considered to represent diameters with significantly different means. The Tukey-Kramer HSD shows that the Small, Medium, and Large nanoparticle have significantly different mean diameters. However, the Small and Medium nanoparticles have only borderline significantly different mean diameters. This is not surprising considering that the Small and Medium nanoparticles are synthesized using the same block copolymer,  $PS_{11000}\text{-}b\text{-}PAA_{1200}$ , only with different metal loadings.

The Tukey-Kramer HSD test in Figure 7 represents the distribution of nanoparticle diameters for Large, Medium, and Small arrays, using circles. The particle counts are; 49 for Small, 187 for Medium, and 151 for Large. The

diameters of the circles represent the distribution of nanoparticle diameters that falls within the 95 % confidence level range. Significantly different distributions are indicated by circles for which the outside angle of intersection is less than or equal to  $90^\circ$ . Circles that intersect at a  $90^\circ$  angle are considered to be borderline significantly different. Using the Tukey-Kramer HSD test it is shown that the Large nanoparticles have a mean diameter that is significantly different from the Small and Medium mean nanoparticle diameters. The Small and Medium nanoparticles have mean diameters which are borderline significantly different. It is not surprising that the Small and Medium nanoparticles have only borderline significantly different mean diameters, because the Small and Medium nanoparticles were synthesized from the same block copolymer,  $PS_{11000}\text{-}b\text{-}PAA_{1200}$ , only with different metal loadings.

That fact that the nanoparticles synthesized from the single block copolymer and single metal loadings systems have mean diameters that are significantly different infers that the mean diameter values calculated for the nanoparticle arrays can be considered distinct from one another. Furthermore, knowing that the single block copolymer and metal loading systems yield nanoparticles with significantly different mean diameters leads to the hypothesis that these single block copolymer and metal loading systems may be combined to produce nanoparticle arrays with diameter distributions that reflect the significantly different mean diameters of their constituents; in other words bimodal nanoparticle arrays.

## 3.2. Single PS-*b*-PAA Block Copolymer and Metal Loading Systems

### 3.2.1. Small

Figure 8 below shows the diameter distribution calculated for the Small (PS<sub>11000</sub>-*b*-PAA<sub>1200</sub> Metal Loading = 0.5) nanoparticles. The total number of particles analyzed was 49. The micelle solution was 0.5 wt%, and had equilibrated for 1 week before this sample was spin cast. A red normal curve was fitted to the distribution of nanoparticle diameters. A normal-quantile plot was produced with the distribution of nanoparticle diameters. As seen in Figure 8, the distribution of nanoparticle diameters falls within the 95% confidence bounds, in red. The distribution of nanoparticle diameters in the normal-quantile plot also fits reasonably well to the straight, red normal-quantile line. These characteristics of the distribution of Small nanoparticle diameters indicate that it is normally distributed. Therefore, a mean nanoparticle diameter can be calculated for the Small nanoparticles. The mean Small nanoparticle diameter is 5.8 nm with a standard deviation of 1.2 nm.

## Small

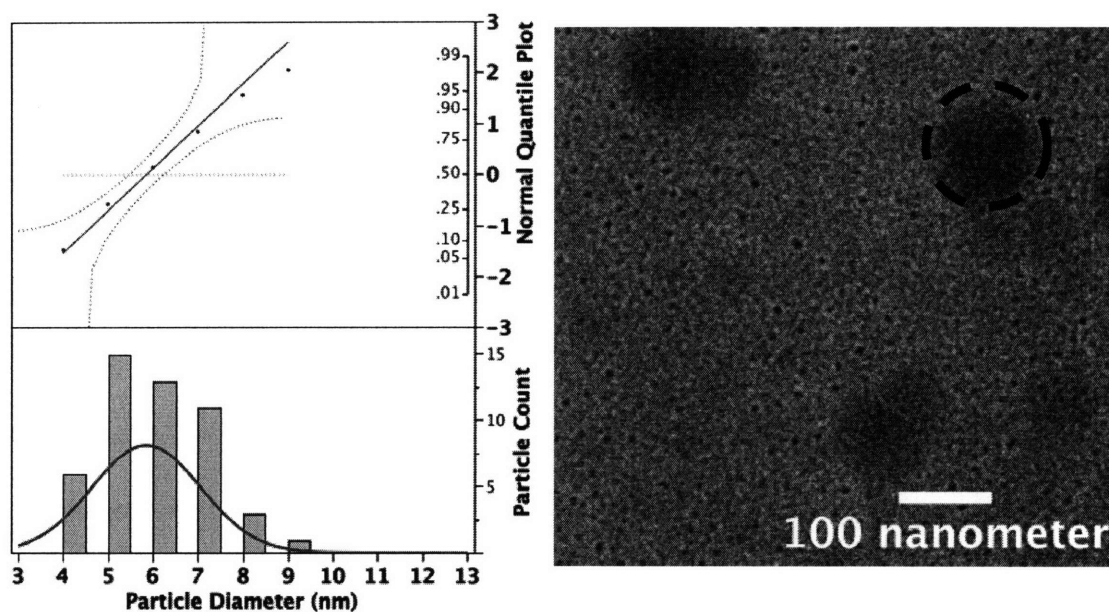


**Figure 8** Distribution of particle diameters for Small ( $\text{PS}_{11000}\text{-}b\text{-PAA}_{1200}$  Metal Loading = 0.5). The total particle count is 49. The normal-quantile plot above the nanoparticle diameter distribution indicates that the diameters are normally distributed. A normal distribution curve was fitted to the Small nanoparticle distribution to give a mean nanoparticle diameter of 5.8 nm with a standard deviation of 1.2 nm. The inset is a representative TEM image of the Small nanoparticle array. The dark blotches, such as the one circled with the dashed line, appear in several TEM images. They did not significantly affect the morphology of the nanoparticles or the particle diameter analysis. The blotches were determined to be due to debris from undissolved polymer in solution or debris ejected onto the backside of the TEM window during the spin casting process.

### 3.2.2. Medium

Figure 9 below shows the diameter distribution calculated for the Medium ( $\text{PS}_{11000}\text{-}b\text{-PAA}_{1200}$  Metal Loading = 5) nanoparticles. The total number of particles analyzed was 187. The block copolymer solution concentration was 0.5 wt%, and had equilibrated for 1 week before this sample was spin cast. A red normal curve was fitted to the distribution of nanoparticle diameters. A normal-

quantile plot was produced with the distribution of nanoparticle diameters. As seen in Figure 9, the distribution of nanoparticle diameters falls within the 95% confidence bounds, in red. The distribution of nanoparticle diameters in the normal-quantile plot also fits reasonably well to the straight, red normal-quantile line. These characteristics of the distribution of Medium nanoparticle diameters indicate that it is normally distributed. Therefore, a mean nanoparticle diameter can be calculated for the Medium nanoparticles. The mean Medium nanoparticle diameter is 6.80 nm with a standard deviation of 2.20 nm.

### Medium

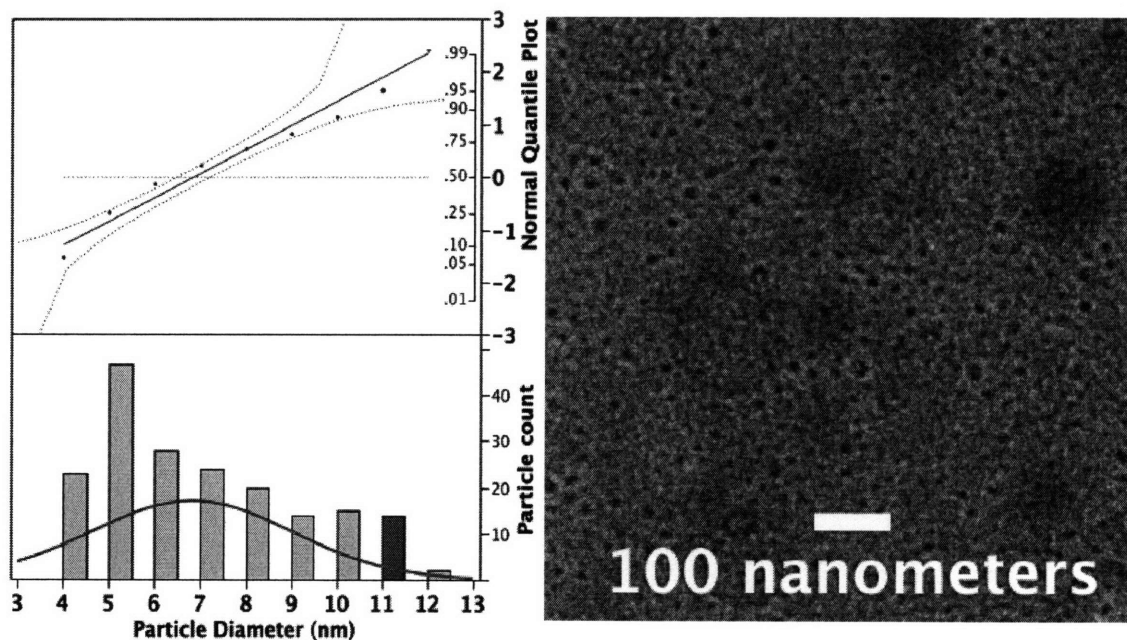


**Figure 9** Distribution of particle diameters for Medium ( $\text{PS}_{11000}\text{-}b\text{-PAA}_{1200}$  Metal Loading = 5). The total particle count is 187 particles. The normal-quantile plot above the nanoparticle diameter distribution indicates that the diameters are normally distributed. A normal distribution curve was fitted to the Medium nanoparticle distribution to give a mean nanoparticle diameter of 6.8 nm with a standard deviation of 2.2 nm. The inset is a representative TEM image of the Medium nanoparticle array.

### 3.2.3. Large

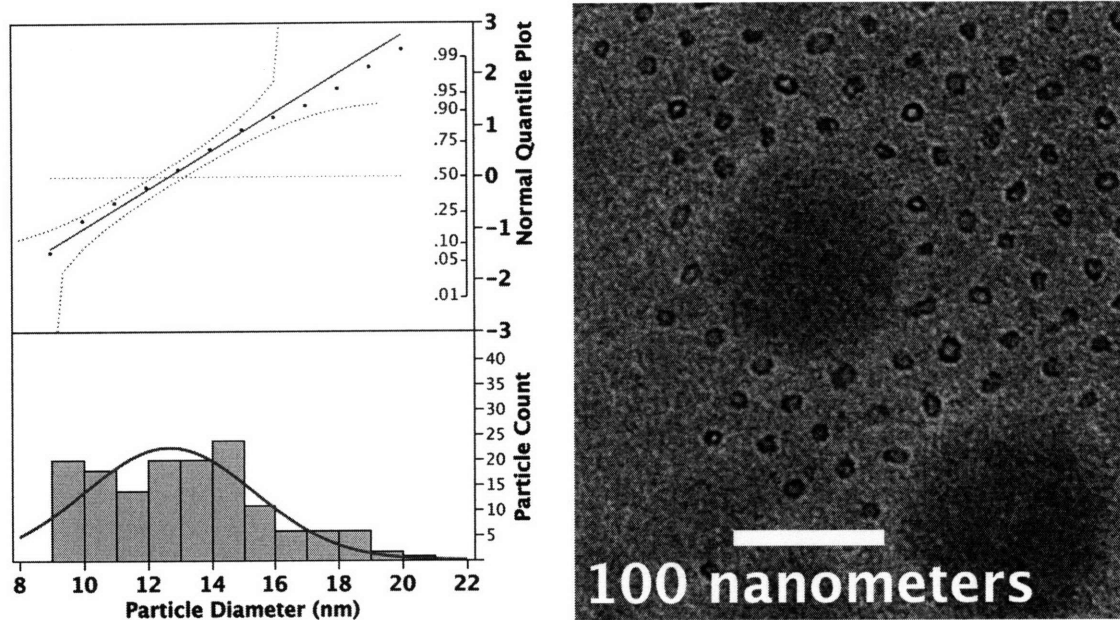
Figure 10 below shows the distribution of particle diameters calculated for the Large (PS<sub>16500</sub>-*b*-PAA<sub>4500</sub> Metal Loading = 5) nanoparticle array. The particle count was 150. A red normal curve was fitted to the distribution of Large nanoparticle diameters. A normal-quantile plot was produced with the distribution of nanoparticle diameters. As seen in Figure 10.

Figure 10 the distribution of nanoparticle diameters falls within the 95% confidence bounds, in red. The distribution of nanoparticle diameters in the normal-quantile plot also fits reasonably well to the straight, red normal-quantile line. These characteristics of the distribution of Large nanoparticle diameters indicate that it is normally distributed. Therefore, a mean nanoparticle diameter can be calculated for the Large nanoparticles. The mean Large nanoparticle diameter is 12.09 nm with a standard deviation of 2.7 nm. The inset TEM in

Figure 10 suggests that the wide range is due to irregularly shaped nanoparticles. In most cases that were observed via TEM the Large solution of nanoparticles was susceptible to stacking through multilayering. The stacked nanoparticles would form irregularly shaped agglomerates after plasma etching. Though that is not considered to be the cause of the irregularly shaped nanoparticles in this particular analysis, because the nanoparticles appear to be regularly spaced and discrete. Attempts were made to decrease the stacking effect by decreasing the concentration of the PS-*b*-PAA block copolymer solution from 0.5 wt% to 0.2 wt%. The Large micelle solution yielded the most hexagonally close-packed array of nanoparticles.



## Large



**Figure 10** Distribution of particle diameters for Large ( $\text{PS}_{16500}\text{-}b\text{-PAA}_{4500}$  Metal Loading = 5). The total particle count is 150. The normal-quantile plot above the nanoparticle diameter distribution indicates that the diameters are normally distributed. A normal distribution curve was fitted to the Large nanoparticle distributions to give a mean nanoparticle diameter of 12.07 nm with a standard deviation of 2.70 nm. The inset is a representative TEM image of the Large nanoparticle array. The hollow appearance of the nanoparticles was determined to be caused by focusing effects in the TEM, and do not reflect a true morphological characteristic of the nanoparticles. Similar conclusions about nanoparticles that appear hollow were reached by Bennett 2007. The spread of the nanoparticle diameter distribution can be attributed to the irregularly shaped Large nanoparticles, as seen in the inset TEM image. In this image it can be seen that the dark blotch due to undissolved polymer debris has caused the nanoparticle array to form around it. While this debris does affect the nanoparticle array, it does not affect the particle diameter analysis or the general modality of the nanoparticle diameters.

### 3.3. Summary of nanoparticle diameters available using single systems of one PS-*b*-PAA block copolymer and one metal loading

Mean nanoparticle diameters and standard deviations were calculated for the nanoparticles synthesized from single PS-*b*-PAA block copolymers and metal loadings: Small, Medium, and Large. These values are shown below in Table 2.

**Table 2 A summary of the mean nanoparticle diameters available, and the standard deviations for the Small, Medium, and Large PS-*b*-PAA block copolymer and metal loading systems is shown below. No data was available for XLarge at the time that this report was written. The XLarge category is included for completeness.**

Single Block Copolymer - Metal Loading Systems					
Relative Size	Block Copolymer	Metal Loading	Mean Diameter (nm)	Mean Diameter Std Dev (nm)	Particle Count
Small	PS <sub>11000</sub> - <i>b</i> -PAA <sub>1200</sub>	0.50	5.80	1.20	49
Medium	PS <sub>11000</sub> - <i>b</i> -PAA <sub>1200</sub>	5.00	6.80	2.20	187
Large	PS <sub>16500</sub> - <i>b</i> -PAA <sub>4500</sub>	5.00	12.07	2.70	151
XLarge	PS <sub>2200</sub> - <i>b</i> -PAA <sub>11500</sub>	5.00	unavailable	unavailable	unavailable

### 3.4. Combinations of Two Block Copolymer and Metal Loading Systems

A priori, it is expected that the number of ‘big’ nanoparticles, in the array produced from combined solutions, would be much less than the number of ‘small’ nanoparticles, because the PS-*b*-PAA micelle and metal loading solutions were prepared with respect to a weight percentage concentration of PS-*b*-PAA block copolymer in toluene. Statistically this weight-averaged concentration does not reflect the number of micelles in solution. Therefore, combining equal volumes of a ‘big’

micelle solution and a ‘small’ micelle solution results in a solution with a number average of micelle sizes that is skewed to a large number of ‘small’ micelles. This ‘small’ micelle rich solution produces nanoparticle arrays that reflect that skew. The particle diameter histograms presented in this section exhibit the expected skew to ‘small’ micelles<sup>§</sup>.

As discussed previously in 3.1, because the Small, Medium, and Large nanoparticle arrays are shown to be normally-distributed and their respective means are significantly different, it can be expected that a combination of the Small and Medium, or Small and Large, and by extension the Small and XLarge block copolymer and metal loading systems will yield nanoparticle diameter distributions that are bimodal. Taken alone, a non-normal nanoparticle distribution is not concrete evidence of bimodality of the physical nanoparticles. However, the nanoparticle distributions represent the physical sizes of the nanoparticles as imaged with TEM. Consulting TEM images of the nanoparticle arrays in conjunction with the nanoparticle diameter distributions lends significant confidence to the conclusions that may be reached using both analyses.

To aid in identifying the single modes of nanoparticle diameter distributions that constitute the nanoparticle diameter distributions, each distribution for Small + Medium, Small + Large, and Small + XLarge have been decomposed. The non-normal nanoparticle distributions have been decomposed into data sets that are normally distributed. The decomposed normally distributed nanoparticle diameter

---

<sup>§</sup> Attempts were made to produce nanoparticle arrays that had a greater number of ‘big’ micelles with respect to the ‘small’ micelles. However these results have not yet shown significant improvement over the particle diameter distributions shown herein.

distributions have mean diameters and standard deviations that represent the unimodal diameter distributions of the constituent single Small, Medium, Large, or XLarge nanoparticles.

#### **3.4.1. Small + Medium**

Figure 11 below shows the distribution of particle diameters calculated for the combined Small (PS<sub>11000</sub>-*b*-PAA<sub>1200</sub> Metal Loading = 0.5) and Medium (PS<sub>11000</sub>-*b*-PAA<sub>1200</sub> Metal Loading = 5) nanoparticle systems. The total particle count is 95. The solutions were 0.5 wt% and had equilibrated for 1 week before spin casting. A normal-quantile plot was produced with the distribution of Small + Medium nanoparticle diameters. As seen in Figure 11 the distribution of nanoparticle diameters does fall within the 95% confidence bounds, in red. However, the distribution of nanoparticle diameters in the normal-quantile plot does not fit well to the straight, red normal-quantile line. These characteristics of the distribution of Small + Medium nanoparticle diameters indicate that it is not normally distributed. Therefore, a mean nanoparticle diameter cannot be calculated for the Small + Medium nanoparticles.

## Small + Medium

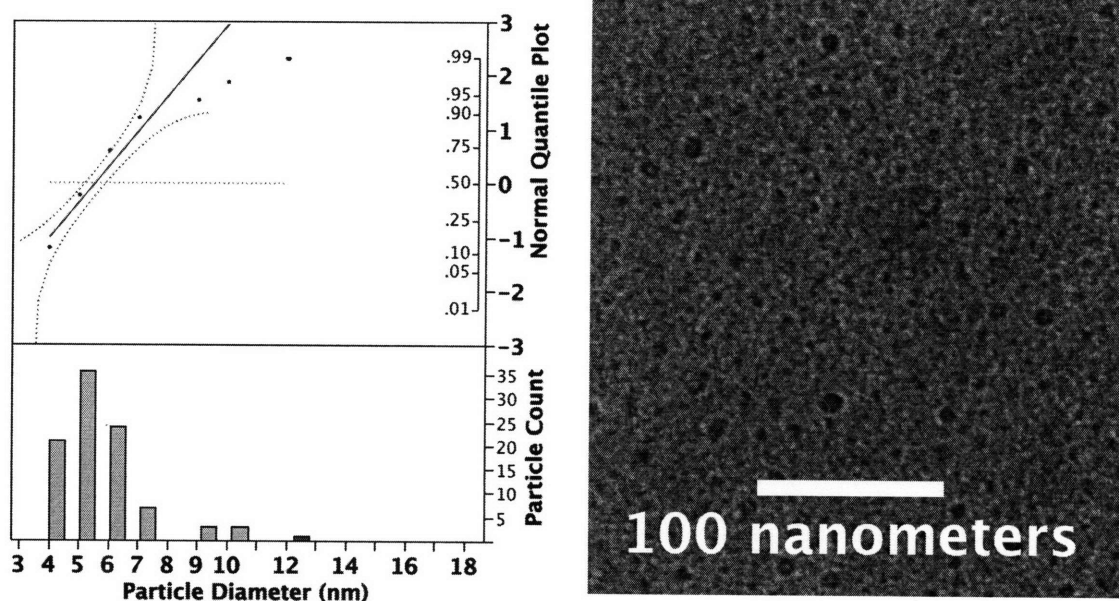


**Figure 11** Distribution of particle diameters for a combined solution of Small and Medium solutions ( $\text{PS}_{11000}\text{-}b\text{-PAA}_{1200}$  Metal Loading = 0.5 +  $\text{PS}_{11000}\text{-}b\text{-PAA}_{1200}$  Metal Loading = 5). The normal-quantile plot above the nanoparticle diameter distribution indicates that the diameters are not normally distributed. The inset is a representative TEM image of the Small + Medium nanoparticle array.

The nanoparticle diameter distribution for the Small + Medium nanoparticles has been decomposed into unimodal constituents that represent the single Small and Medium nanoparticles. The decomposed diameter distributions are shown below in Figure 12. The decomposed unimodal diameter distributions represent true constituent distributions of the combined bimodal Small + Medium distribution. The normal-quantile plots for each decomposed unimodal diameter distribution shows that the distribution is normally distributed. The mean and standard deviations for the decomposed Small and Medium distributions are  $5.19 \text{ nm} \pm 0.89 \text{ nm}$  and  $9.8 \text{ nm} \pm 1.06 \text{ nm}$ , respectively. The standard deviations of the decomposed Small and Medium distributions overlap with the standard

deviations of the single Small and Medium nanoparticle diameter distributions calculated in 3.2. The fact that the standard deviations for the decomposed Small distributions overlap, and the standard deviations for the decomposed Medium distributions overlap indicates that the decomposed Small and Medium distributions reflect the unimodal Small and Medium constituents.

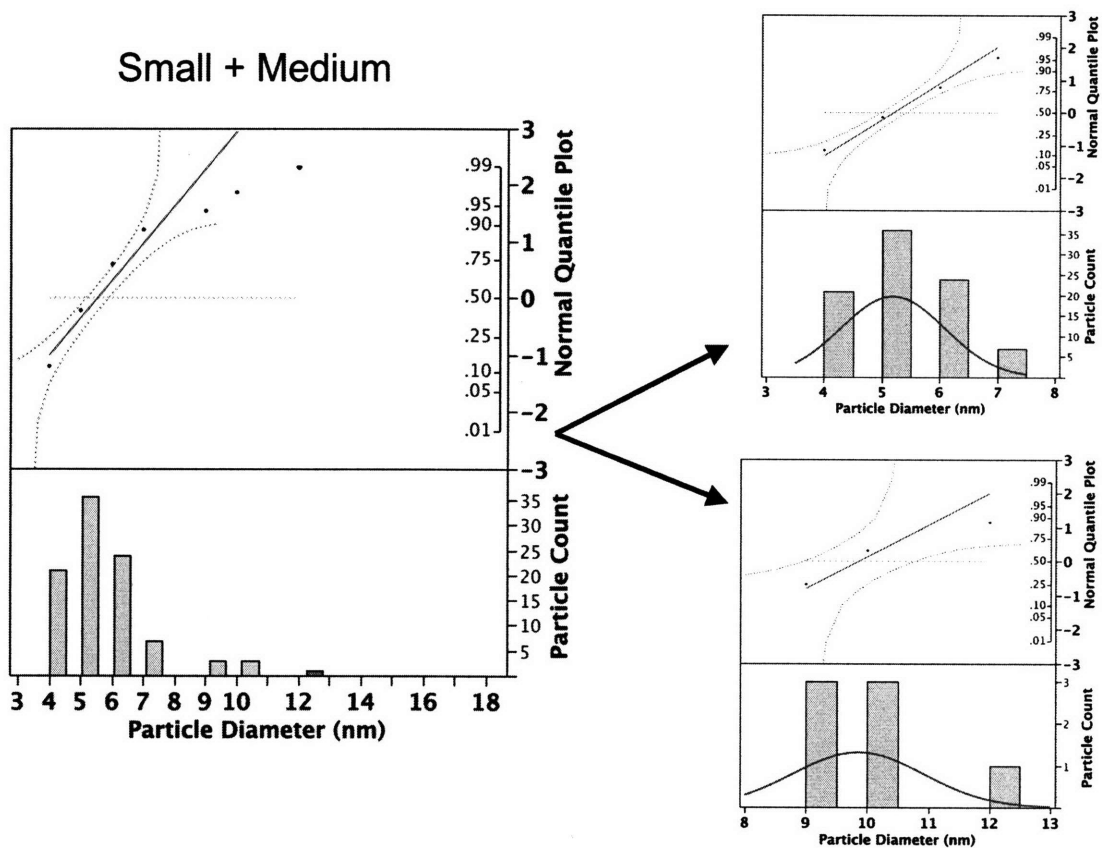


**Figure 12** The unimodal nanoparticle diameter distributions that constitute the non-normal Small + Medium nanoparticle diameter distribution are shown extracted to the right. The unimodal nanoparticle diameter distributions are normally distributed with means and standard deviations of  $5.19 \text{ nm} \pm 0.89 \text{ nm}$  for the top distribution and  $9.8 \text{ nm} \pm 1.06 \text{ nm}$  for the bottom distribution. The unimodal nanoparticle diameter distributions represent the Small and Medium constituents of the Small + Medium nanoparticle diameter distribution because the standard deviations for the Small distributions overlap and the standard deviations for the Medium distributions overlap.

### 3.4.2. Small + Large

Figure 13 below shows the distribution of particle diameters calculated for the combined Small (PS<sub>11000</sub>-*b*-PAA<sub>1200</sub> Metal Loading = 0.5) and Large (PS<sub>16500</sub>-*b*-PAA<sub>4500</sub> Metal Loading = 5) nanoparticle systems. The total particle count is 97. The solutions were 0.5 wt% and had equilibrated for 4 months before spin casting. A normal-quantile plot was produced with the distribution of nanoparticle diameters. As seen in Figure 13 the distribution of nanoparticle diameters does not fall completely within the 95% confidence bounds, in red. The distribution of nanoparticle diameters in the normal-quantile plot does not fit well to the straight, red normal-quantile line. These characteristics of the distribution of Small + Large nanoparticle diameters indicate that it is not normally distributed. Therefore, a mean nanoparticle diameter cannot be calculated for the Small + Large nanoparticles.

## Small + Large

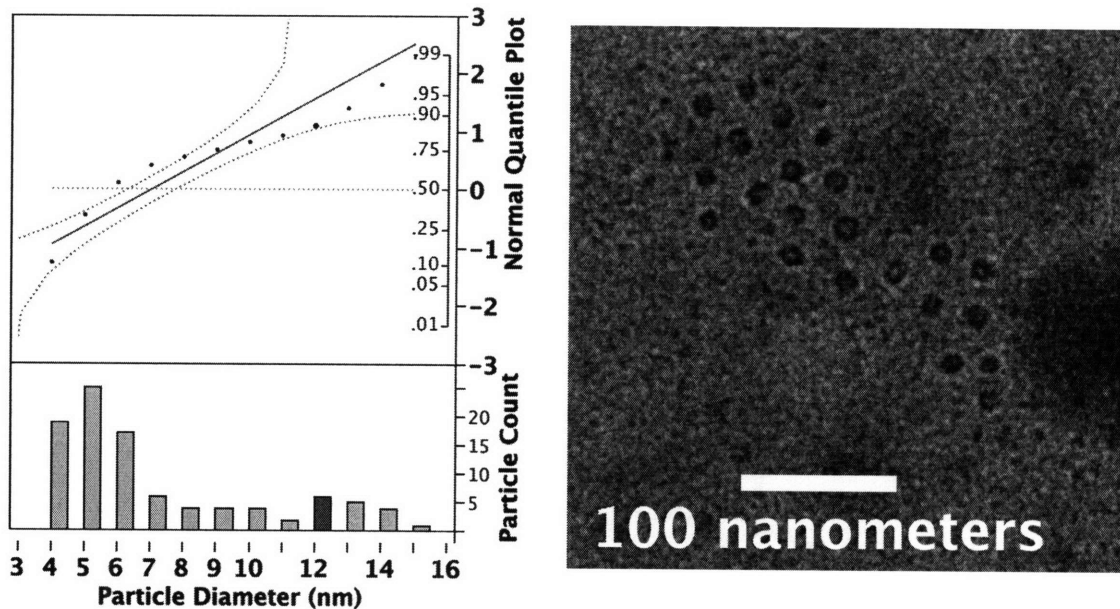


**Figure 13 Distribution of particle diameters for a combined solution of Small and Large solutions (PS<sub>11000</sub>-*b*-PAA<sub>1200</sub> Metal Loading = 0.5 + PS<sub>16500</sub>-*b*-PAA<sub>4500</sub> Metal Loading = 5). The total particle count is 97 particles. The normal-quantile plot above the nanoparticle diameter distribution indicates that the diameters are not normally distributed. The inset is a representative TEM image of the Small + Large nanoparticle array.**

The nanoparticle diameter distribution for the Small + Large nanoparticles has been decomposed into unimodal constituents that represent the single Small and Large nanoparticles. The decomposed diameter distributions are shown below in Figure 14. The decomposed unimodal diameter distributions represent the constituent distributions of the combined bimodal Small + Large distribution. The normal-quantile plots for each decomposed unimodal diameter distribution shows that the distribution is normally distributed. The mean and standard deviations for the decomposed Small and Large distributions are 5.50 nm ± 1.40 nm and 11.70 nm ± 1.80 nm, respectively. The standard



deviations of the decomposed Small and Large distributions overlap with the standard deviations of the single Small and Large nanoparticle diameter distributions calculated in 3.2. The fact that the standard deviations for the decomposed Small distributions overlap, and the standard deviations for the decomposed Large distributions overlap indicates that the decomposed Small and Large distributions reflect the unimodal Small and Large constituents.

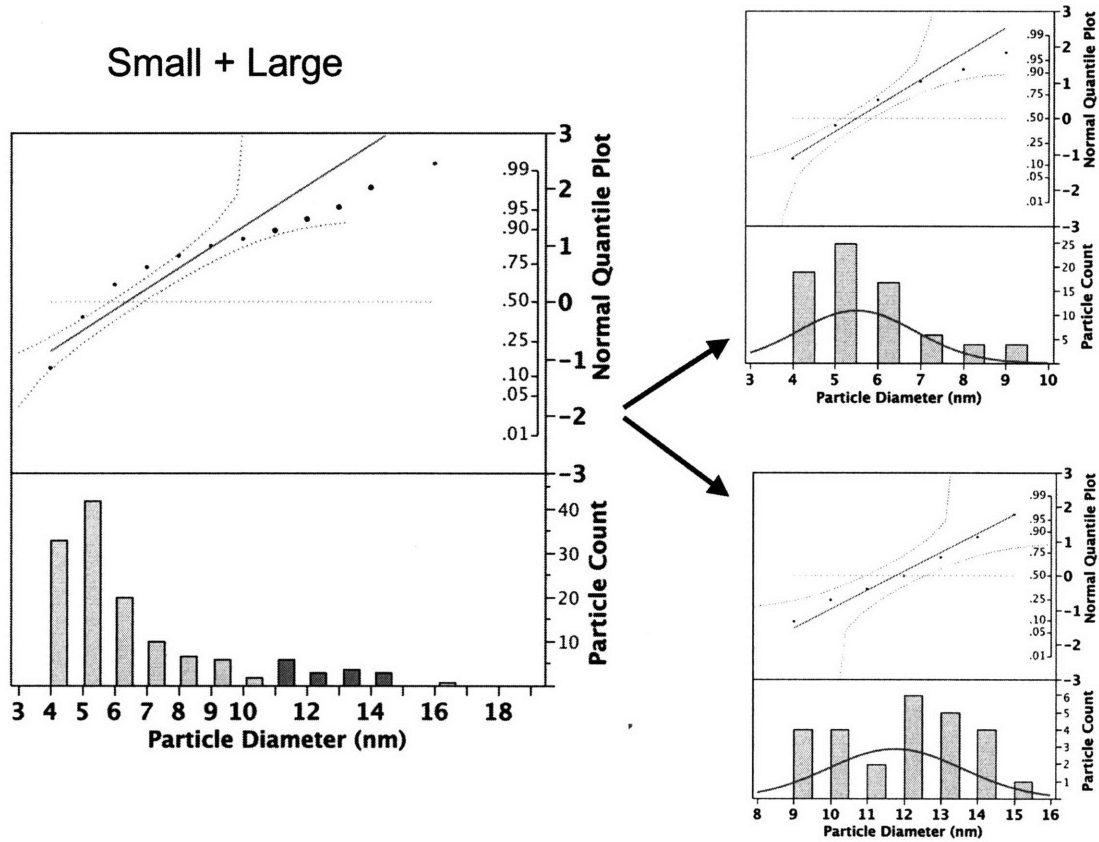


**Figure 14** The unimodal nanoparticle diameter distributions that constitute the non-normal Small + Large nanoparticle diameter distribution are shown extracted to the right. The unimodal nanoparticle diameter distributions are normally distributed with means and standard deviations of  $5.55 \text{ nm} \pm 1.40 \text{ nm}$  for the top distribution and  $11.70 \text{ nm} \pm 1.80 \text{ nm}$  for the bottom distribution. The unimodal nanoparticle diameter distributions represent the Small and Large constituents of the Small + Large nanoparticle diameter distribution because the standard deviations for the Small distributions overlap and the standard deviations for the Large distributions overlap.

### 3.4.3. Small + XLarge

Figure 15 below shows the histogram of particle diameters calculated for the combined Small (PS<sub>11000</sub>-*b*-PAA<sub>1200</sub> Metal Loading = 0.5) and XLarge (PS<sub>2200</sub>-*b*-PAA<sub>11500</sub> Metal Loading = 5) nanoparticle systems. The total particle count is 137. The solutions were 0.2 wt% and had equilibrated for 1 week before spin casting. A normal-quantile plot was produced with the distribution of nanoparticle diameters. As seen in Figure 15 the distribution of nanoparticle diameters does not fall completely within the 95% confidence bounds, in red. The distribution of nanoparticle diameters in the normal-quantile plot does not fit well to the straight, red normal-quantile line. These characteristics of the distribution of Small + XLarge nanoparticle diameters indicate that it is not normally distributed. Therefore, a mean nanoparticle diameter cannot be calculated for the Small + XLarge nanoparticles.

## Small + XLarge

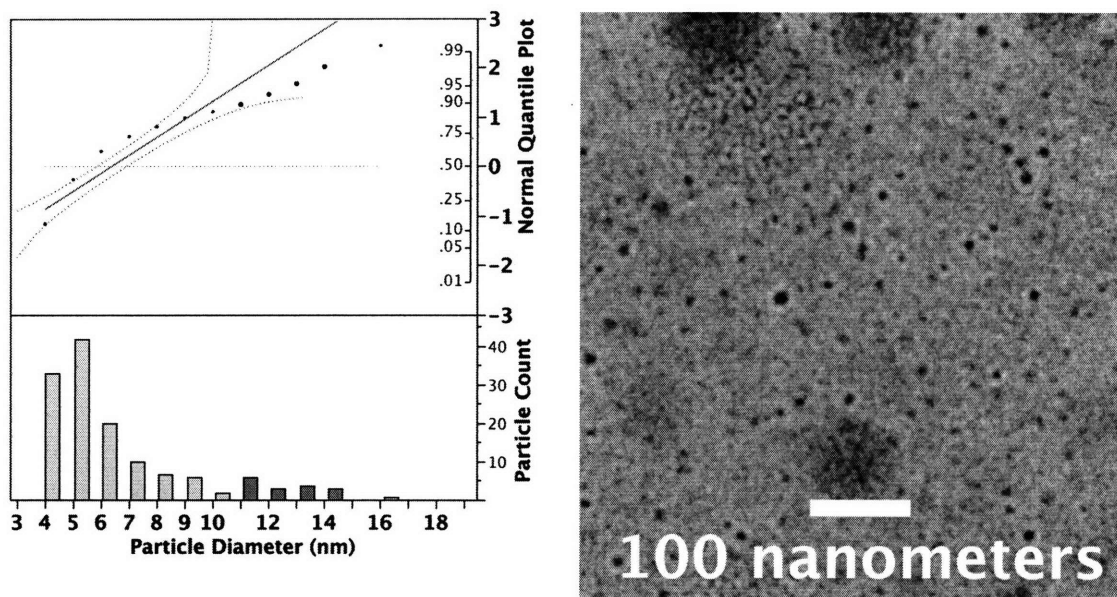


**Figure 15 Distribution of particle diameters for a combined solution of Small and XLarge solutions (PS<sub>11000</sub>-*b*-PAA<sub>1200</sub> Metal Loading = 0.5 + PS<sub>2200</sub>-*b*-PAA<sub>11500</sub> Metal Loading = 5). The total particle count is 137 particles. The normal-quantile plot above the nanoparticle diameter distribution indicates that the diameters are not normally distributed. The inset is a representative TEM image of the Small + XLarge nanoparticle array.**

The nanoparticle diameter distribution for the Small + XLarge nanoparticles has been decomposed into unimodal constituents that represent the single Small and XLarge nanoparticles. The decomposed diameter distributions are shown below in Figure 16. The decomposed unimodal diameter distributions represent the constituent distributions of the combined bimodal Small + XLarge distribution. The normal-quantile plots for each decomposed unimodal diameter distribution shows that the distribution is normally distributed. The mean and standard deviations for the decomposed Small and XLarge distributions are 5.51 nm  $\pm$  1.50 nm and 12.47 nm  $\pm$  1.47 nm, respectively. The standard deviation of the

decomposed Small distribution overlaps with the standard deviation of the single Small nanoparticle diameter distribution calculated in 3.2. The fact that the standard deviation for the decomposed Small distributions overlap, and that a unimodal distribution corresponding to the XLarge nanoparticles can be extracted indicates that the decomposed Small and XLarge distributions reflect the unimodal Small and XLarge constituents.

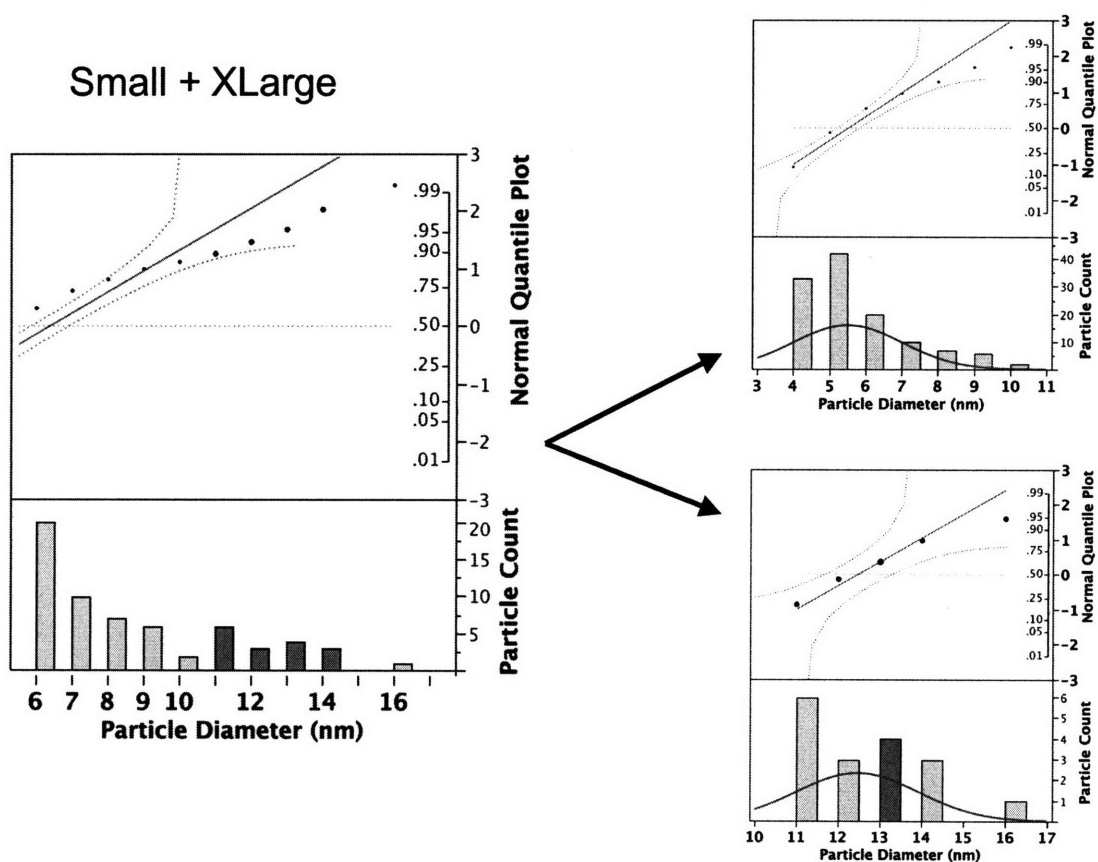


**Figure 16** The unimodal nanoparticle diameter distributions that constitute the non-normal Small + XLarge nanoparticle diameter distribution are shown, extracted to the right. The unimodal nanoparticle diameter distributions are normally distributed with means and standard deviations of  $5.55 \text{ nm} \pm 1.40 \text{ nm}$  for the top distribution and  $12.47 \text{ nm} \pm 1.46 \text{ nm}$  for the bottom distribution. The unimodal nanoparticle diameter distributions represent the Small and XLarge constituents of the Small + XLarge nanoparticle diameter distribution.

### **3.5. Additive Relationship between single and combined systems.**

The particle diameter distributions of the single block copolymer and metal loading systems that constitute the combined block copolymers and metal loadings systems are superimposed to qualitatively determine if an additive relationship exists between the single systems and their combinations.

#### **3.5.1. Small, Medium, and Small + Medium**

In Figure 17 below, the Small and Medium nanoparticle diameter distributions are superimposed on the combined Small + Medium nanoparticle diameter distribution. The distribution for the Small nanoparticle array is indicated with a thin dashed line, and has a mean diameter of 5.8 nm with a standard deviation of 1.2 nm. The distribution for the Medium nanoparticle array is indicated with a thick dashed line, and has a mean diameter of 6.8 nm with a standard deviation of 2.2 nm. The distribution for the combined Small + Medium nanoparticle array is indicated with a thick solid line. As discussed in 3.4, the nanoparticle diameter distribution for the Small + Medium nanoparticles can be decomposed into two unimodal diameter distributions. The decomposed unimodal distributions of Small + Medium have a low mean of 5.19 nm with a standard deviation of 0.89 nm, and a high mean of 9.8 nm with a standard deviation of 1.06 nm. The low and high unimodal means correspond to the means of the single Small and Medium diameter distributions, with standard deviations that overlap. These overlapping standard deviations indicate that an additive relationship exists for the Small, Medium, and combined nanoparticle arrays of Small + Medium.

This additive relationship effectively results in a bimodal dispersion of Small and Medium nanoparticles when they are combined.

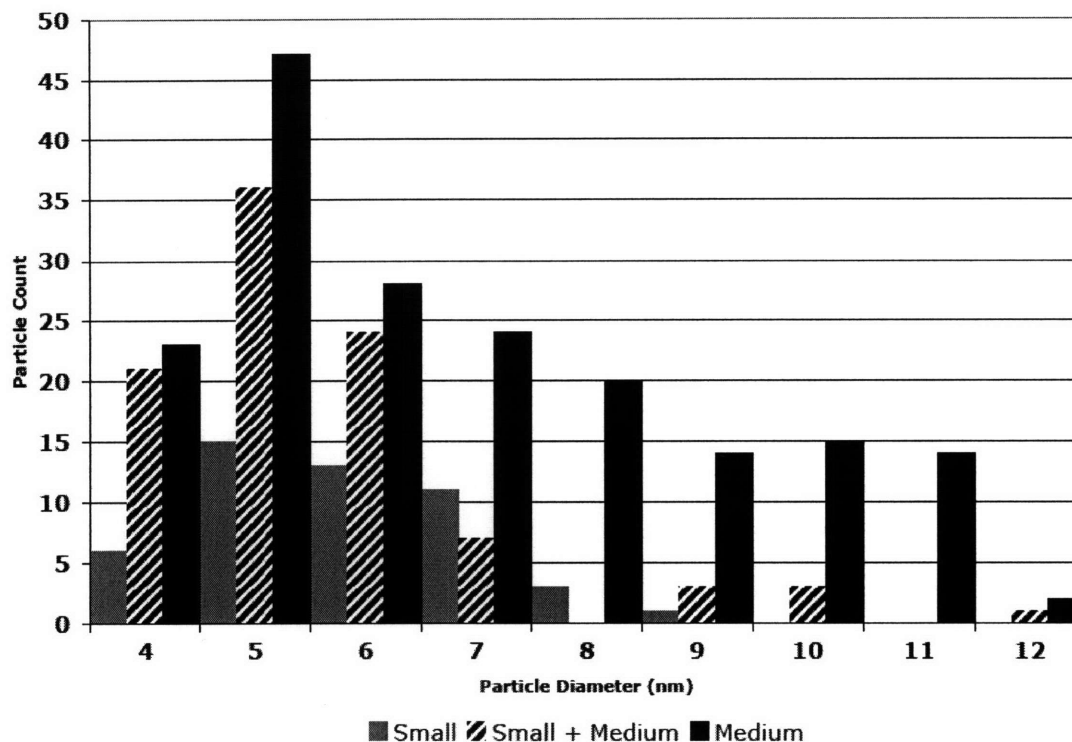


**Figure 17** A superposition of the single Small and Medium diameter distributions, and the Small + Medium diameter distribution is shown. The diameter distribution for the Small nanoparticles is indicated in gray, and has a mean diameter of 5.8 nm with a standard deviation of 1.2 nm. The diameter distribution for the Medium nanoparticles is indicated in black, and has a mean diameter of 6.8 nm with a standard deviation of 2.2 nm. The diameter distribution for the combined Small + Medium nanoparticles is indicated in diagonal black lines. The decomposed unimodal distributions of Small + Medium have a low mean of 5.19 nm with a standard deviation of 0.89 nm, and a high mean of 9.8 nm with a standard deviation of 1.06 nm. The low and high unimodal means correspond to the means of the single Small and Medium diameter distributions, with standard deviations that overlap.

### 3.5.2. Small, Large, and Small + Large

In Figure 18 below, the Small and Large nanoparticle diameter distributions are superimposed on the combined Small + Large nanoparticle diameter distribution. The distribution for the Small nanoparticle array is indicated with a thin dashed line, and has a mean diameter of 5.80 nm with a standard deviation of 1.20 nm. The distribution for the Large nanoparticle array is indicated with a thick dashed line, and has a mean diameter of 12.09 nm with a standard deviation of 2.70 nm. The distribution for the combined Small + Large nanoparticle array is indicated with a thick solid line. As discussed in 3.4, the nanoparticle diameter distribution for the Small + Large nanoparticles can be decomposed into two unimodal diameter distributions. The decomposed unimodal distributions of Small + Large have a low mean of 5.50 nm with a standard deviation of 1.4 nm, and a high mean of 11.70 nm with a standard deviation of 1.80 nm. The low and high unimodal means correspond to the means of the single Small and Large diameter distributions, with standard deviations that overlap. These overlapping standard deviations indicate that an additive relationship exists for the Small, Large, and combined nanoparticle arrays of Small + Large. This additive relationship effectively results in a bimodal dispersion of Small and Large nanoparticles when they are combined.

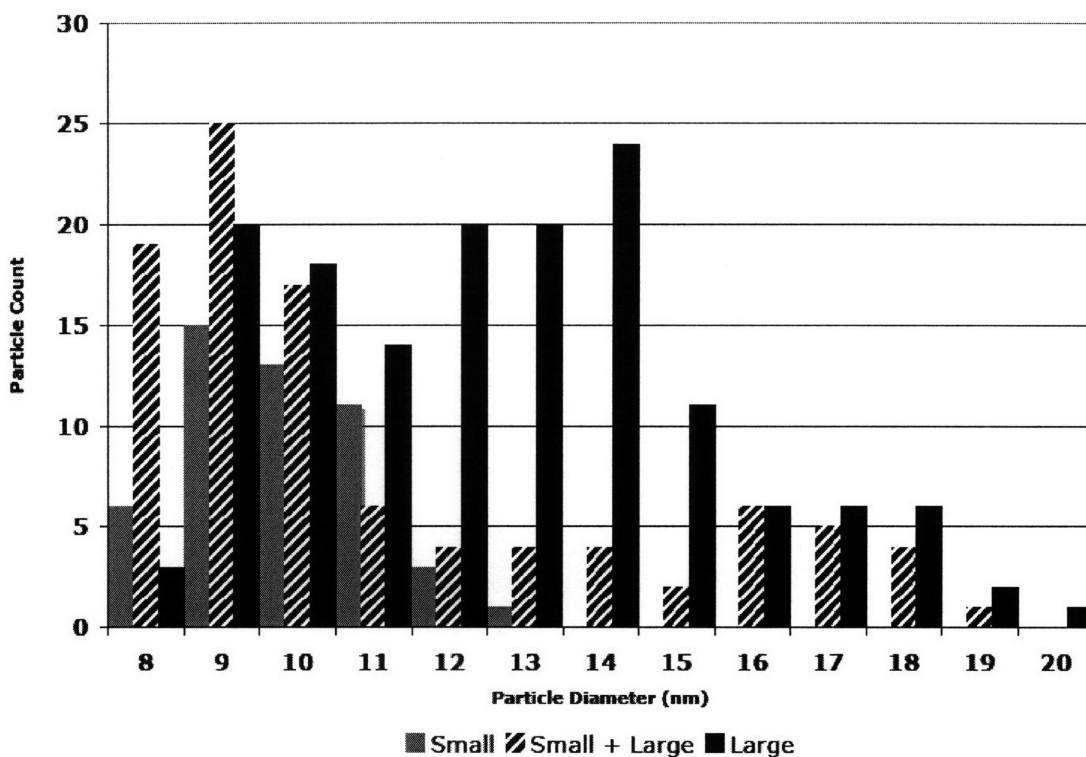


Figure 18 A superposition of the single Small and Large diameter distributions, and the Small + Large diameter distribution is shown. The diameter distribution for the Small nanoparticles is indicated in gray, and has a mean diameter of 5.80 nm with a standard deviation of 1.20 nm. The diameter distribution for the Large nanoparticles is indicated in black, and has a mean diameter of 12.09 nm with a standard deviation of 2.70 nm. The diameter distribution for the combined Small + Large nanoparticles is indicated in diagonal black lines. The decomposed unimodal distributions of Small + Large have a low mean of 5.50 nm with a standard deviation of 1.40 nm, and a high mean of 11.70 nm with a standard deviation of 1.80 nm. The low and high unimodal means correspond to the means of the single Small and Large diameter distributions, with standard deviations that overlap.

### 3.5.3. Small, and Small + XLarge

In Figure 19 below, the Small nanoparticle diameter distributions is superimposed on the combined Small + XLarge nanoparticle diameter distribution. No diameter distribution was calculated for a XLarge nanoparticle



array because suitable samples were not obtained. XLarge samples often had agglomerates of block polymer on the sample surface. The surface debris produced poor samples even after etching away polymer in oxygen plasma. The distribution for the Small nanoparticle array is indicated with a thin dashed line, and has a mean diameter of 5.8 nm with a standard deviation of 1.2 nm. The distribution for the combined Small + XLarge nanoparticle array is indicated with a thick solid line. As discussed in 3.4, the nanoparticle diameter distribution for the Small + XLarge nanoparticles can be decomposed into two unimodal diameter distributions. The decomposed unimodal distributions of Small + XLarge have a low mean of 5.51 nm with a standard deviation of 1.50 nm, and a high mean of 12.47 nm with a standard deviation of 1.46 nm. The low and high unimodal means correspond to the means of the single Small and XLarge diameter distributions, with standard deviations that overlap for Small diameter nanoparticles. These overlapping standard deviations indicate that an additive relationship exists for the Small, XLarge, and combined nanoparticle arrays of Small + XLarge. This additive relationship effectively results in a bimodal dispersion of Small and XLarge nanoparticles when they are combined.

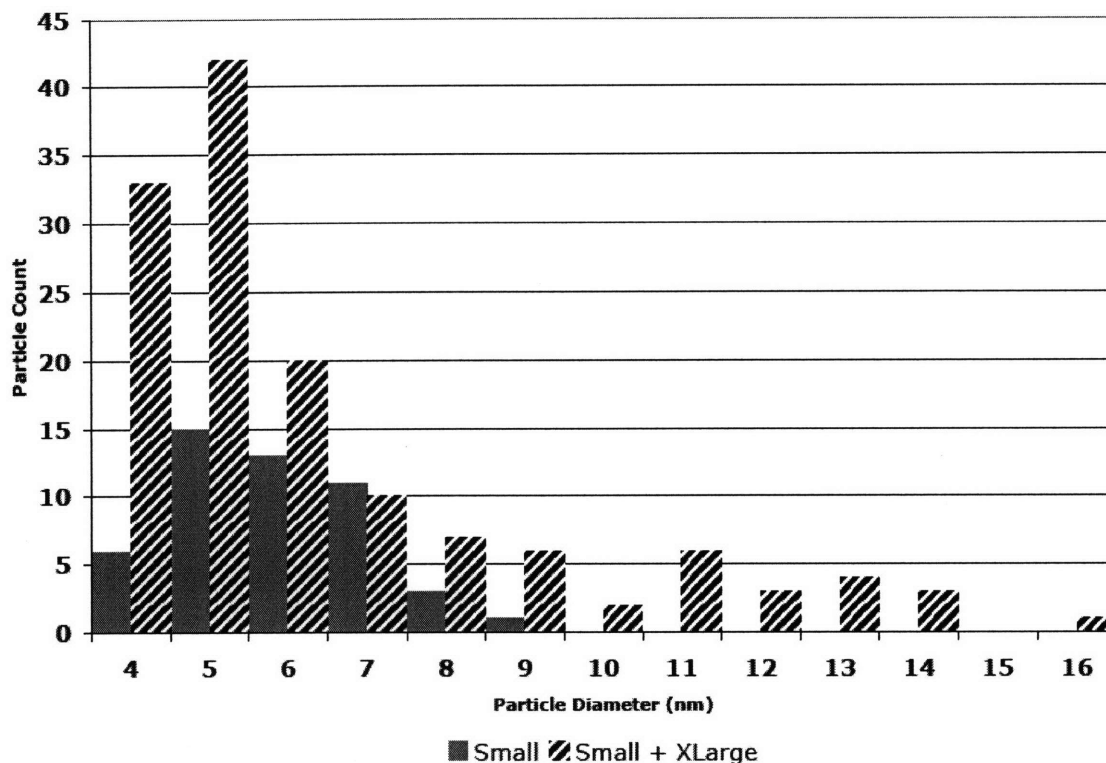


Figure 19 An overlay of the single solution Small, and the combined solution Small + XLarge histograms is shown. The diameter distribution for the Small nanoparticles is indicated in gray and has a mean diameter of 5.80 nm with a standard deviation of 1.20 nm. The diameter distribution for the combined Small + XLarge nanoparticles is indicated in diagonal black lines. The decomposed unimodal distributions of Small + XLarge have a low mean of 5.51 nm with a standard deviation of 1.50 nm, and a high mean of 12.47 nm with a standard deviation of 1.46 nm. The low and high unimodal means correspond to the means of the single Small and XLarge diameter distributions, with standard deviations that overlap for the Small diameter nanoparticles.

### 3.6. Summary of nanoparticle diameters available using additive system of nanoparticle arrays

Table 3 below gives the mean nanoparticle diameters that are available using the combined nanoparticle arrays analyzed above. It should be noted that the particle counts for certain decomposed unimodal diameter distributions are not statistically

significant. Future analyses over several more nanoparticle arrays will serve to produce more statistically significant particle counts. However, the mean diameter distributions are observed to accurately reflect the distribution of nanoparticle diameters that is observed in TEM. Combining this approximate statistical analysis with the physical relevance of TEM for the nanoparticle arrays lends confidence to the values presented in Table 3.

**Table 3 The peak nanoparticle diameters available for a combined set of block copolymers and metal loadings are indicated in the table.**

Combined Block Copolymer - Metal Loading Systems					
Relative Sizes	Block Copolymers	Metal Loading	Mean Diameter (nm)	Mean Diameter Std Dev (nm)	Particle Count
Small	PS <sub>11000</sub> - <i>b</i> -PAA <sub>1200</sub>	0.50	5.19	0.89	88
Medium	PS <sub>11000</sub> - <i>b</i> -PAA <sub>1200</sub>	5.00	9.80	1.06	7
Small	PS <sub>11000</sub> - <i>b</i> -PAA <sub>1200</sub>	0.50	5.50	1.40	75
Large	PS <sub>16500</sub> - <i>b</i> -PAA <sub>4500</sub>	5.00	11.70	1.80	26
Small	PS <sub>11000</sub> - <i>b</i> -PAA <sub>1200</sub>	0.50	5.51	1.50	120
XLarge	PS <sub>2200</sub> - <i>b</i> -PAA <sub>11500</sub>	5.00	12.47	1.46	17

### 3.7. Factors affecting the nanoparticle diameter distributions

The mean nanoparticle diameters for the decomposed unimodal Medium and Large are greater than the mean diameters of the single Medium and the single Large nanoparticle diameter distributions. In other words, the Medium and Large nanoparticles have a greater mean diameter when combined with the Small nanoparticles, rather than when they are spin cast as single nanoparticle arrays of

just Medium or just Large. It is expected that micelles in solution ripen according to a fundamental driving force to reduce free energy via a reduction in surface area.<sup>15</sup>

Two mechanisms are thought to control dynamic size equilibrium of the metal-loaded micelles.<sup>15,16</sup> The first mechanism is a relatively rapid inter-micellular diffusion of the metal species at room temperature (27 °C). Extended periods of mixing (> 5 seconds) of two micelle solutions that have different metal loadings are thought to produce micelles with homogenized amounts of metal species. The results of this inter-micellular diffusion of metal species can be seen in poorly spin cast nanoparticle arrays of combined solutions. The second mechanism is inter-micellular diffusion of individual block copolymers. This mechanism is thought to take place over larger time scales (~ hours) at room temperature (27 °C).<sup>16</sup>

Micelle ripening in the combined Small + Medium, Small + Large, and Small + XLarge solutions analyzed in this report most likely occurs through the mechanism of rapid inter-micellular diffusion of metal species. This mechanism should result in combined micelle solutions which produce nanoparticles with a decomposed unimodal diameter distribution, corresponding to the larger nanoparticles, which have mean diameters greater than the mean diameters of those same larger nanoparticles when they are not spin cast in combination. This is the result that is found for the decomposed unimodal diameter distributions in Small + Medium, Small + Large, and Small + XLarge. Micelle ripening caused by the second mechanism of inter-micellular diffusion of block copolymers is not

considered for the nanoparticle arrays analyzed in this report, because the combined nanoparticle arrays and their constituent single nanoparticle arrays were spin cast after equilibrating for about the same time (e.g. 1 week, 4 months, 5 months). Future studies of metal-loaded PS-*b*-PAA block copolymer micelles will be aimed at investigating the kinetics of the second ripening mechanism.

### **3.8. Grazing Incidence Small-angle X-ray Scattering (GISAXS) of Nanoparticle Arrays**

Figure 20 below shows a representative GISAXS image of a Large nanoparticle array. The bright horizontal intensities to the right of the beam stop is scattering from the structure factor of the Large nanoparticle array. The structure factor scattering is related to the inter-particle spacing, and is indicated with a black arrow. Appendix B provides more information about the inter-particle spacings recently measured using GISAXS.

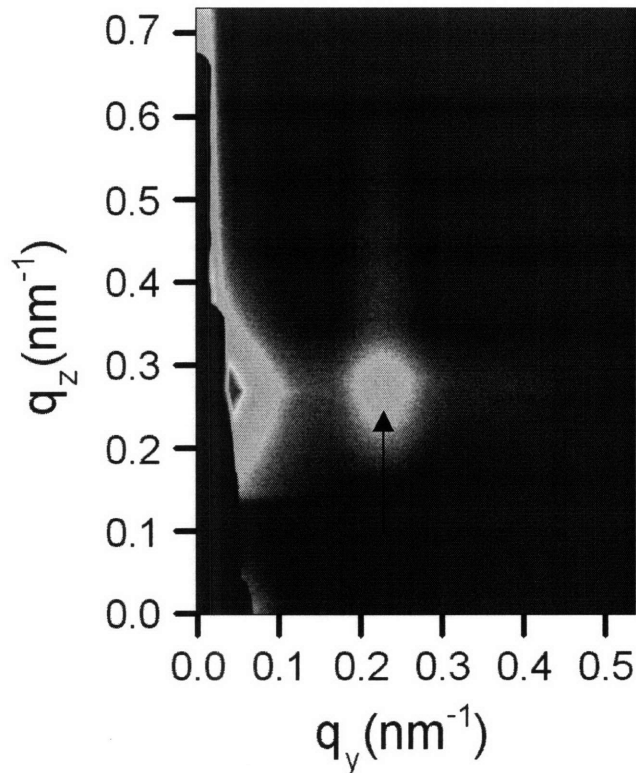


**Figure 20** A representative grazing incidence small-angle X-ray scattering (GISAXS) image taken of nanoparticle array. Structure factor scattering related to spacing between the nanoparticles is indicated with a black arrow.

Figure 21 below is a plot of a series of GISAXS intensities collected for a Large nanoparticle array as it was heated from room temperature to 820 °C. The heating is similar to the heating step described in Section 2.5. The heating step is common for all carbon nanotube growth protocols and is referred to as annealing. It was necessary to plot the GISAXS intensities through the annealing of the PS-*b*-PAA-templated nanoparticles so that a comparison could be made between the thermal characteristics of this type of nanoparticle array and the typical metallic nanoparticle array that is used to catalyze carbon nanotube growth. In this case, Figure 21 shows that the structure factor peak, indicated with a black arrow, begins to disappear as the nanoparticle array is heated. This indicates that the inter-particle spacing of the nanoparticles becomes less periodic

through the annealing process, and suggests that, in annealing, the PS-*b*-PAA-templated nanoparticles rearrange slightly. \*\*

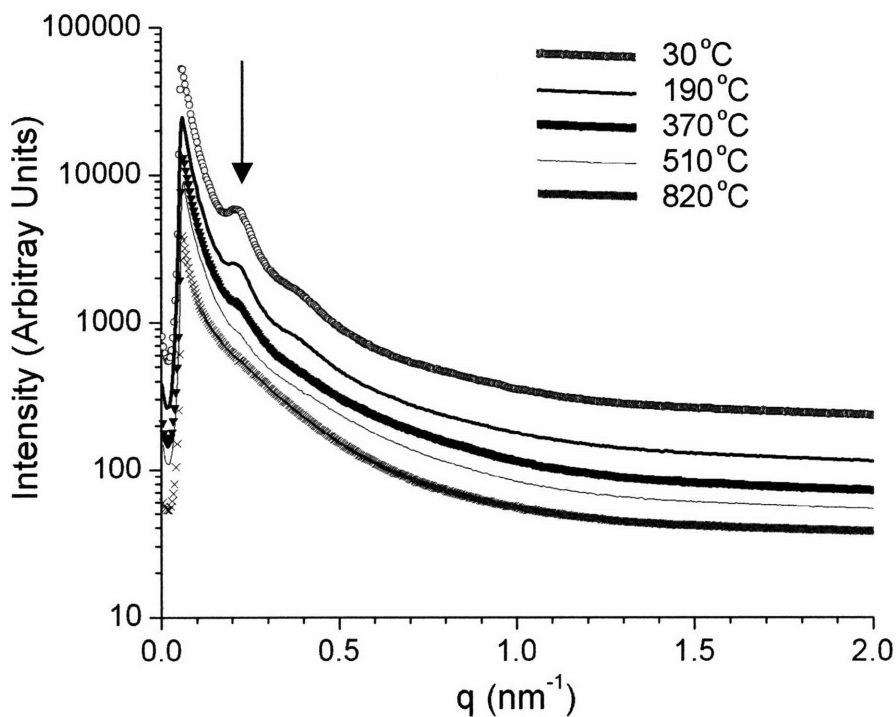


**Figure 21** GISAXS intensities for a Large nanoparticle array that is heated from room temperature (30 °C) to the typical carbon nanotube growth temperature (820 °C) are shown. This process is termed annealing. Annealing is performed routinely on metallic nanoparticle arrays used for catalyzing carbon nanotube growth. The structure factor peak is indicated with a black arrow. It can be seen that the intensity of the structure factor peak disappears as the Large nanoparticle array is annealed. This indicates a slight rearrangement of the nanoparticles.

---

\*\* Studies aimed at investigating the high temperature rearrangement of the nanoparticles are currently underway. Surface stresses and near atomic level imperfections in the sample substrate may cause the nanoparticles to rearrange in an effort to find the lowest energy positions available.

### 3.9. Small-Angle X-ray Scattering of Carbon Nanotubes Grown From Nanoparticle Arrays

Only the 0.2 wt % Large and the 0.2 wt% XLarge diameter nanoparticle arrays were able to catalyze carbon nanotube growth. Figure 22 shows a SAXS image for a typical carbon nanotube forest grown from a Large diameter nanoparticle array.

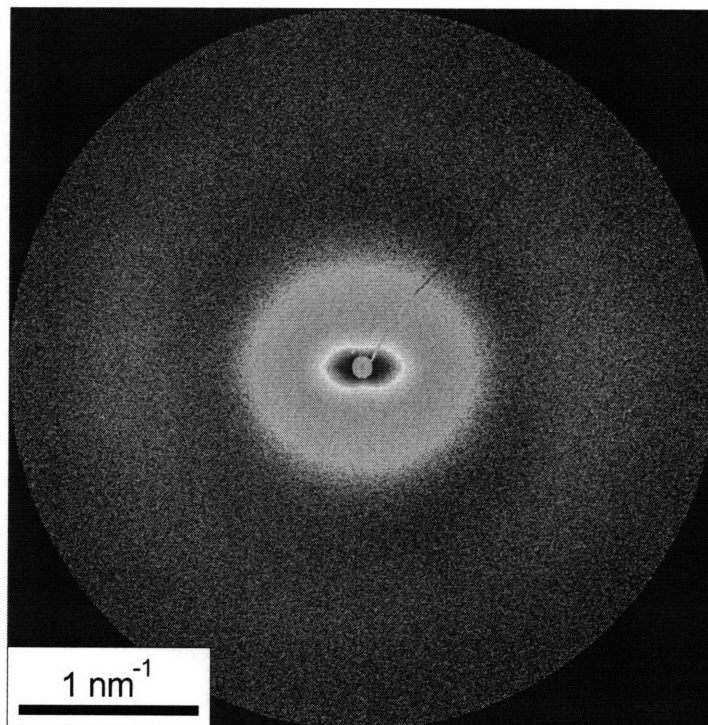


**Figure 22** A small-angle X-ray scattering (SAXS) image of a carbon nanotube forest grown from a Large diameter nanoparticle array. The SAXS image indicates vertical alignment for the carbon nanotube forest.

The SAXS image indicates the carbon nanotube forest is vertically aligned. This is indicated by the diffuse intensities at the right and left of the beam stop. Figure 23 shows an analysis of SAXS intensities taken from a progressive vertical scan of a carbon nanotube forest grown from a Large diameter carbon nanotube forest.



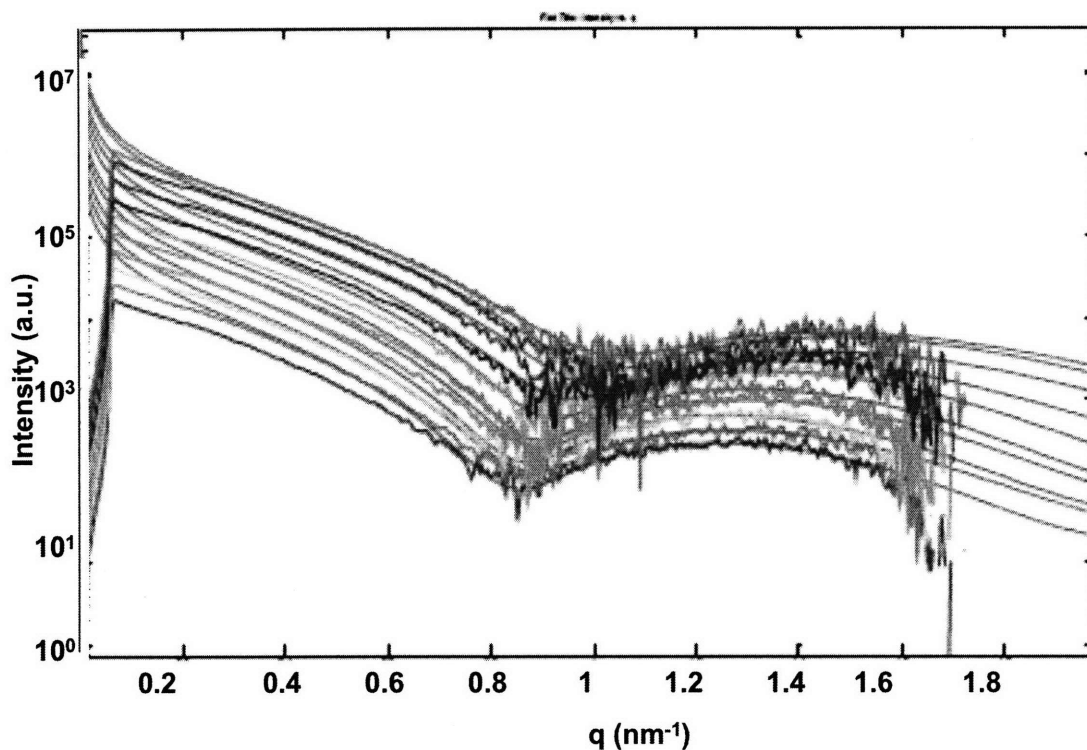


**Figure 23 SAXS intensities for a carbon nanotube forest grown from an array of Large diameter nanoparticles. For this analysis  $c = 0.5$ , the average diameter was 6.9 nm, the standard deviation was 0.82 nm, and the Hermans orientation factor was 0.52.**

A significant amount of noise is present in higher  $q$  range of the intensities. However that did not prevent an analysis of the intensities. The ratio of carbon nanotube inner diameter to outer diameter used to analyze the SAXS intensities was  $c = 0.5$ . The Hermans orientation factor was 0.52. The average diameter was 6.9 nm, with a standard deviation of 0.82 nm. Figure 24 below shows a TEM image of carbon nanotubes grown from a Large diameter nanoparticle array.

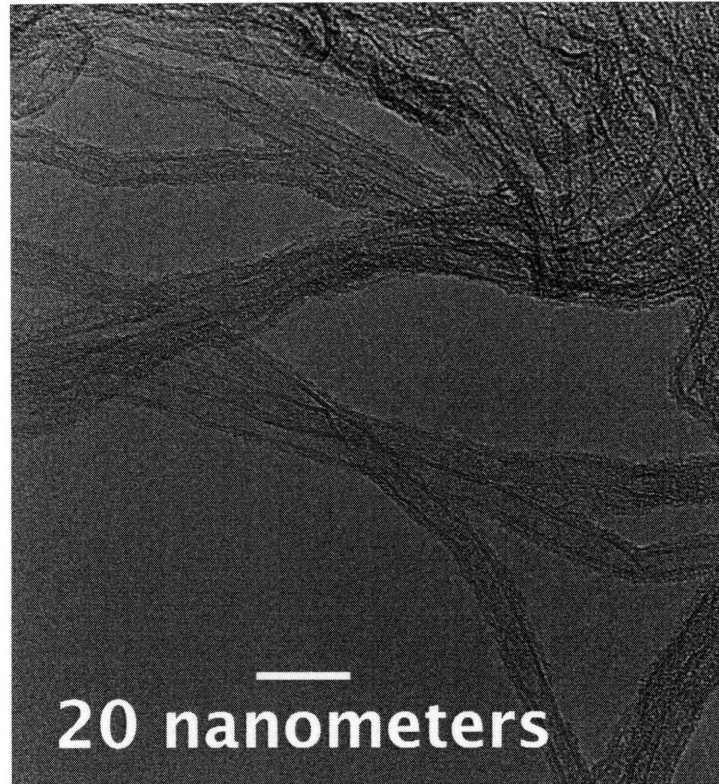


**Figure 24 TEM image of carbon nanotubes grown from a Large diameter nanoparticle array. SAXS analysis indicated that the carbon nanotubes grown from the Large diameter nanoparticle arrays had an average diameter of 6.9 nm with a standard deviation of 0.82 nm. The Hermans orientation factor was 0.52. The carbon nanotubes are supported on a holey carbon film.**

Figure 23 below shows SAXS intensities collected for a progressive vertical scan of a carbon nanotube forest grown from a XLarge nanoparticle array. For this analysis  $c = 0.7$ , the average diameter was 6.4 nm, the standard deviation was 1.2 nm, and the Hermans orientation factor was close to 0.

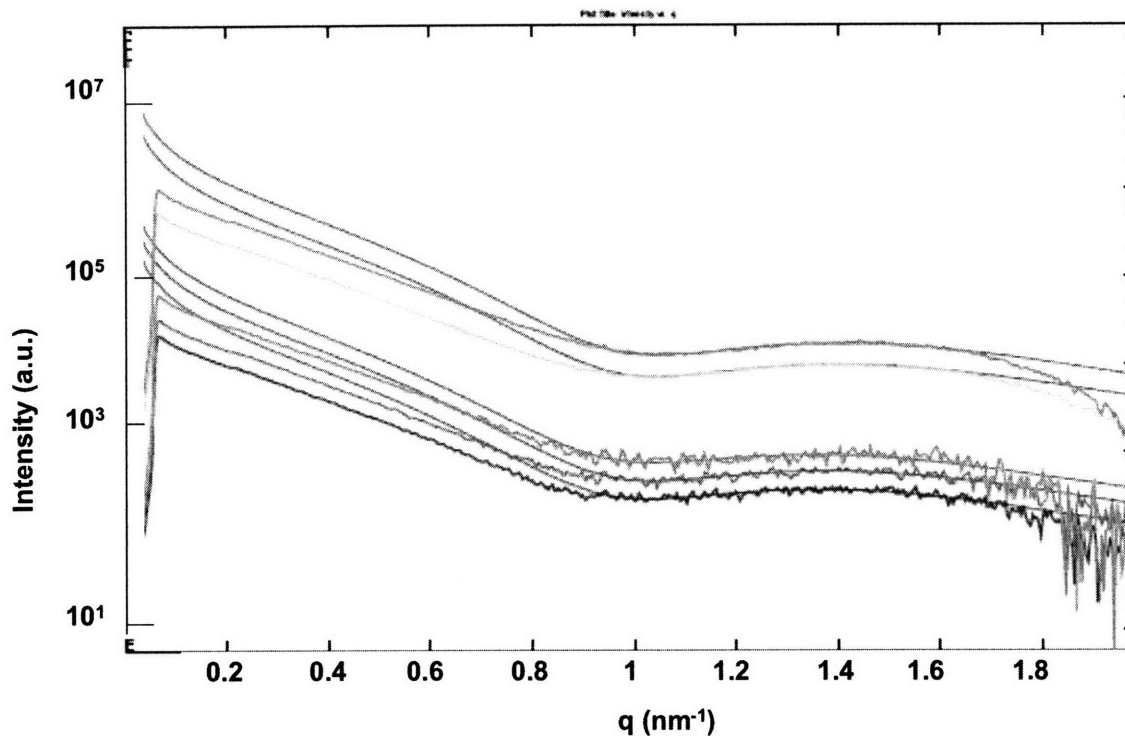


**Figure 25 SAXS intensities for a carbon nanotube forest grown from an array of XLarge diameter nanoparticles. For this analysis  $c = 0.7$ , the average diameter was 6.4 nm, the standard deviation was 1.2 nm, and the Hermans orientation factor was close to 0.**

The SAXS analysis showed that the carbon nanotubes grown from the Large and XLarge nanoparticle arrays had a low standard deviation for the measured diameters. The SAXS analysis indicated that the Large diameter nanoparticle arrays produced carbon nanotubes with diameters that were larger than the carbon nanotubes produced by the XLarge diameter nanoparticle array. The difference calculated with SAXS is 0.5 nm. The fact that the XLarge nanoparticles had a larger mean diameter than the Large nanoparticles, but produced carbon nanotubes with average diameters that were smaller than the average diameters for carbon nanotubes grown from the Large nanoparticles is not contradictory. That is because, at this point the growth mechanism of carbon nanotubes catalyzed on inorganic nanoparticles is not fully understood.

#### 4. Summary and Conclusions

Carbon nanotubes have unique material properties that make them incredibly desirable for several applications including: composite reinforcement, nanoelectronics, novel sensors, biomaterials, etc. Making full use of the unique properties that carbon nanotubes have requires precise control of their crystalline structure. Defects<sup>††</sup>, carbon nanotube chirality, carbon nanotube diameter, and number of walls are just some of the physical characteristics of carbon nanotubes that directly affect their unique properties.

In this report it has been shown that PS-*b*-PAA block copolymer templated inorganic nanoparticle catalysts offer substantial control over the diameters of carbon nanotubes grown from them. The distribution of diameters of nanoparticles formed using PS-*b*-PAA block copolymer micelles loaded with Fe<sup>3+</sup> metal species were calculated from TEM images taken of the nanoparticle arrays. An extensive survey of many TEM images ensured that the images used for statistical analysis were representative of typical nanoparticle arrays. The distributions of diameters of nanoparticles formed from combinations of different molecular weight PS-*b*-PAA block copolymers and different metal loadings (referred to according to relative size as Small, Medium, and Large) were shown to be significantly different. A fourth size of nanoparticle, XLarge, was used in this study, but lack of sample availability prevented statistical analysis for the single XLarge nanoparticles.

---

<sup>††</sup> See Appendix A for a TEM image of a carbon nanotube defect.

A hypothesis was made that a combination of the significantly different nanoparticle diameter distributions of Small, Medium, Large, or XLarge would result in an array of nanoparticles with a bimodal distribution of nanoparticle diameters. This was found to be true, and the resulting bimodal distributions of nanoparticle diameters were decomposed into unimodal diameter distributions. The unimodal diameter distributions were found to be normally distributed with mean diameters and standard deviations that overlapped with the mean diameters and standard deviations of the single Small, Medium, and Large nanoparticles.

GISAXS studies performed on the PS-*b*-PAA block copolymer templated nanoparticles show that the nanoparticles have periodic spacing. TEM images of the nanoparticle arrays also show that the nanoparticles are regularly spaced. In fact, the Large nanoparticles show hexagonal close packing. GISAXS studies performed on nanoparticle arrays undergoing annealing showed that the nanoparticles lost periodic spacing during annealing. This is thought to be due to the nanoparticles rearranging themselves, with respect to near atomic level substrate imperfections or surface stresses, in an effort to find the lowest energy positions available. This finding is significant to consider when precise placement of carbon nanotubes is required, e.g. in nanoelectronic components. While the nanoparticle spacing is periodic to begin with, annealing would result in a slight rearrangement of the nanoparticles, and correspondingly too, a slightly less well defined spacing of carbon nanotubes.

Carbon nanotubes could only be grown from nanoparticles with larger diameters, such as the Large and XLarge nanoparticles. Small, Medium, and combinations of Small + Medium, Small + Large, and Small + XLarge did not grow using a block

copolymer concentration of 0.2 wt%. The poor growth results are thought to be due to the low (0.2 wt%) concentration that would produce a lower areal density of nanoparticles. The nanoparticle catalysts then have a lower activity, as activity is directly related to areal density.

Small-angle X-ray scattering (SAXS) studies of the carbon nanotube forests grown from the Large nanoparticle arrays indicate a low standard deviation for carbon nanotube diameter, and a reasonable amount of vertical alignment with a Hermans orientation parameter of 0.5. SAXS studies of the carbon nanotube forests grown from the XLarge nanoparticle arrays also indicate a low standard deviation for carbon nanotube diameter, but with almost no alignment. Bennett et al. 2006 showed that lower areal density of nanoparticles results in carbon nanotube forests with less alignment. The nearly non-existent alignment of the carbon nanotube forest grown from the low concentration (0.2 wt%) XLarge nanoparticle arrays agrees with Bennett et al.'s general conclusions.

Several techniques and statistical analyses lead to the conclusion that different sizes of PS-*b*-PAA block copolymer micelles loaded with metal species can be combined to produce bimodal nanoparticle arrays. The quality of carbon nanotube growth from these bimodal nanoparticle arrays is greatly affected by the concentration of metal-loaded micelles in solution. The low standard deviation of carbon nanotube diameters grown from the nanoparticle arrays proves that the PS-*b*-PAA block copolymer micelles offer an excellent means for producing carbon nanotubes with controlled diameters.

The results of recent carbon nanotube growth studies involving the PS-*b*-PAA templated nanoparticles spin cast using higher concentration (0.5 wt%) solutions are provided in Appendix C. The results indicate that the 0.5 wt% combination of Small + XLarge do not produce carbon nanotube forests with bimodal nanoparticle arrays. The other combinations that were analyzed, Small + Medium and Small + Large, did not grow carbon nanotube forests that were dense enough to produce significant SAXS intensities. This latest series of experiments using nanoparticle arrays spin cast from 0.5 wt% solutions addresses a problem identified earlier when attempts were made to grow carbon nanotube forests from nanoparticle arrays that were spin cast from 0.2 wt% solutions. In 3.9 it was found that the 0.2 wt% nanoparticle arrays did not grow carbon nanotube forests well. Only the nanoparticle arrays with the larger particles, Large and XLarge, were able to grow carbon nanotubes. It was concluded that this poor carbon nanotube growth capability was the result of a low areal density of nanoparticles that was due to the low (0.2 wt%) solution concentration. In general, these results indicate that the Small and Medium nanoparticles do not catalyze significant carbon nanotube growth with the gas flow rates and temperature range used, either as single nanoparticle arrays spin cast from 0.2 wt% solutions, or in combination with Large or XLarge nanoparticles spin cast from 0.5 wt% solutions. In the latter case, the lack of bimodality with respect to carbon nanotube diameter indicates that the Small nanoparticles did not catalyze carbon nanotube growth. Future experiments seeking bimodal carbon nanotube forests would benefit from utilizing combined nanoparticle arrays of Large and XLarge, because Large and XLarge nanoparticle arrays showed the best carbon nanotube growth capabilities

throughout all growth experiments conducted in this study. Future experiments would also benefit from exploring the gas flow rates and temperature ranges under which the smaller size nanoparticle can catalyze carbon nanotube growth.



## References

1. Rao, C.N.R.; F.R.S.; Govindaraj, A. *Nanotubes and Nanowires*. RSC Publishing, Cambridge, UK **2005**.
2. Wang, Benjamin N.; Bennett, Ryan D.; Verploegen, Eric; Hart, Anastasios J.; and Cohen, Robert E. *J. Phys. Chem. C* **2007**, 111, 5859-5865
3. Dai, H. *Acc. Chem. Res.* **2002**, 35, 1035-1044.
4. Bennett, R. D.; Hart, A.J.; Cohen, R.E. *Adv. Mater.* **2006**, 18, 2274-2279.
5. Bennett, R. D.; Xiong, G. Y.; Ren, Z. F.; Cohen, R. E. *Chem. Mater.* **2004**, 16, 5589-5595.
6. Seymour, Raymond B. and Carraher, Charles E. *Structure-Property Relationships in Polymers*. Plenum Press, New York, **1984**.
7. Fasolka, Michael J. and Mayes, Anne M. *Annu. Rev. Mater. Res.* **2001**. 31:323–55
8. Liveri, Vincenzo T. *Controlled Synthesis of Nanoparticles in Microheterogeneous Systems*. Springer, New York **2006**
9. Carotenuto, Gianfranco and Nicolais, Luigi *Metal-polymer Nanocomposites*. Wiley-Interscience, Hoboken, NJ **2004**
10. Heilmann, A. *Polymer Films with Embedded Metal Nanoparticles*. Springer, New York **2003**
11. Bennett, Ryan D. *Block Copolymer Thin Forests as Templates for the Production of Tunable Inorganic Nanocluster Arrays and Their Applications*. PhD dissertation, Massachusetts Institute of Technology. **2007**
12. Smilgies, Detlef-M. "GISAXS." June 2007. CHESS. 11 Dec. **2007**  
<<http://staff.chess.cornell.edu/~smilgies/gisaxs/GISAXS.php>>.

13. Verploegen, Eric. *Morphology and Self-Assembly Behavior of Side Chain Liquid Crystalline Block Copolymers*. PhD dissertation, Massachusetts Institute of Technology. **2008**
14. Woehrle, Gerd H.; Hutichison, James E.; Ozkar, Saim; and Finke, Richard G. *Turk J Chem* **2006**, 30, 1-13
15. Ratke, L. and Voorhees, P.W. *Growth and Coarsening*. Springer, New York **2002**
16. Cantu, L.; Corti, M.; and Salina, P. *J. Phys. Chem.* **1991**, 95 5981-5983

## Appendix A: Defect In Multi-walled Carbon Nanotube Imaged Using TEM

Figure 26 below shows a TEM image of a defect in a multiwalled carbon nanotube. This is not a nanotube grown from a PS-*b*-PAA block copolymer templated nanoparticle. This image is a good example of the kinds of defects that limit the ultimate strength of carbon nanotubes. Defects such as this are the hurdles that carbon nanotube synthesis routes such as PS-*b*-PAA block copolymer templated nanoparticles attempt to address.

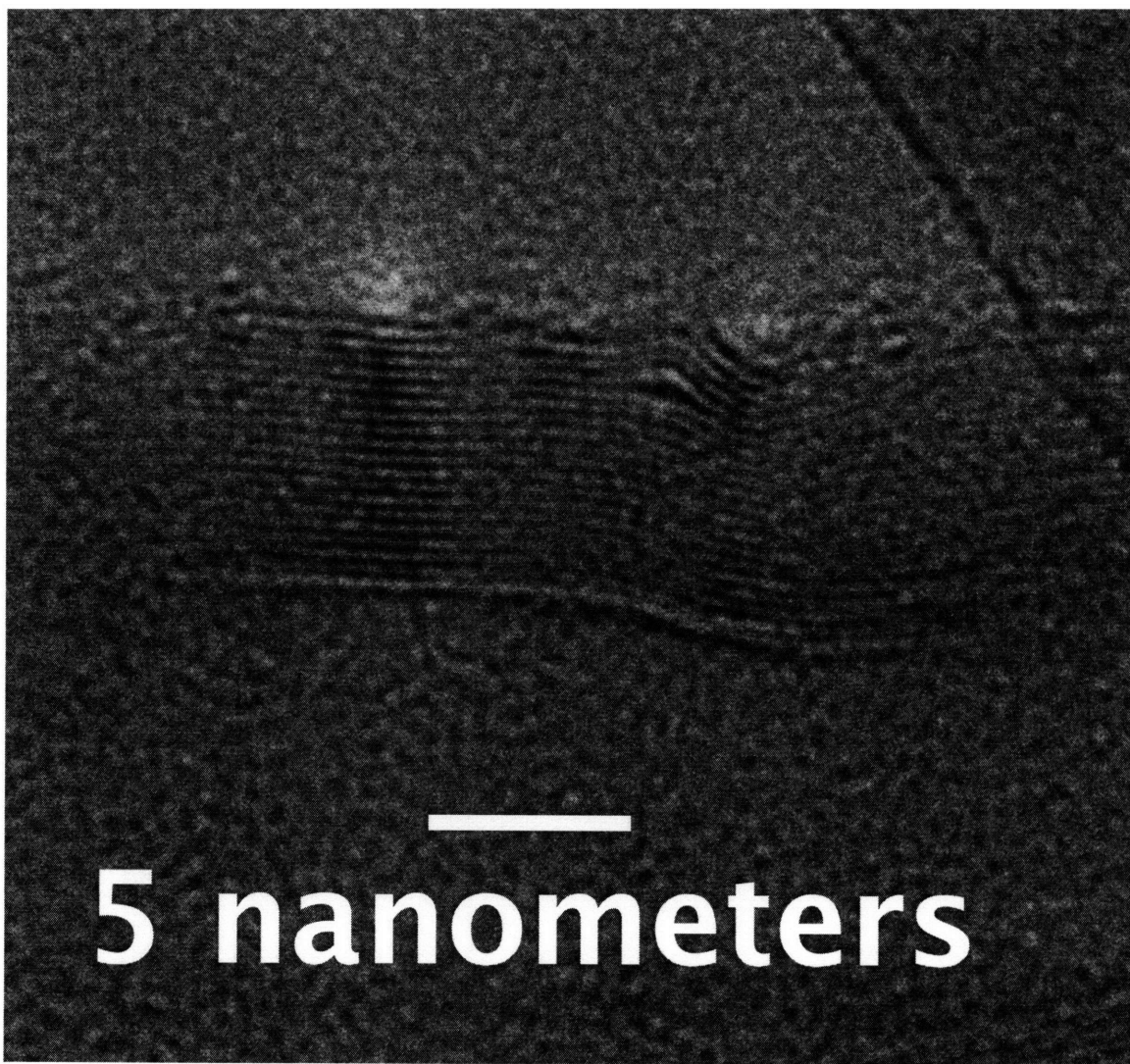
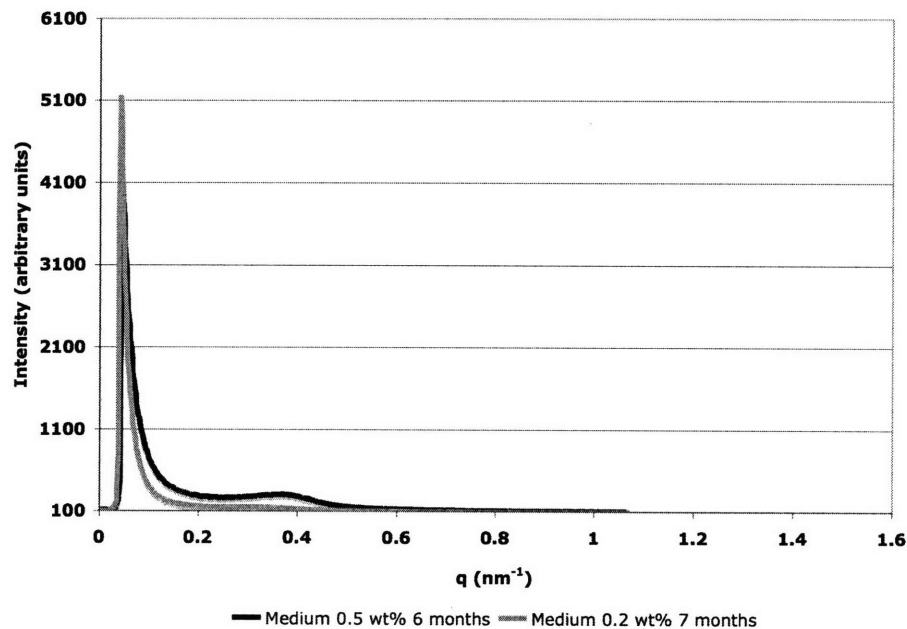


Figure 26 A defect in the walls of a multi-walled carbon nanotube.

## **Appendix B: Inter-particle Spacing of Nanoparticles Spin Cast From 0.5 wt% Solutions**

GISAXS measurements were recently performed on Small, Medium, Large, XLarge, and the combinations Small + Medium, Small + Large, and Small + XLarge. Two samples of each nanoparticle array were spin cast. One sample was a 0.5 wt% solution, and the other sample was a 0.2 wt% solution. There is a 1 month difference in equilibration time for the solutions, before they were spin cast. Below are the results of the GISAXS measurements. Data is only presented for the Medium, Large, and Small + Large nanoparticle arrays of 0.5 wt% and 0.2 wt% concentration. The remaining nanoparticle arrays did not provide sufficient GISAXS intensities to calculate the inter-particle spacing. It should be noted that the inter-particle spacing is only derived from an approximation of the peak value for the GISAXS intensity corresponding to the structure factor scattering intensity. For less sharp peaks, this approximation involves a good deal of subjective fitting. Therefore, the values presented for the inter-particle spacing should be considered to involve a error of  $\pm 2$  nm. This error makes the inter-particle spacing for the Large 0.5 wt% and 0.2 wt% nanoparticle arrays seem equal. The error also makes the inter-particle spacing for the Small + Large 0.5 wt% and 0.2 wt% nanoparticle arrays seem equal. This suggests that differences in equilibration time, up to 1 month, and differences in PS-*b*-PAA block copolymer concentration within the range of 0.2 wt% - 0.5 wt% do not greatly affect the inter-particle spacing of the nanoparticles. Examination of the TEM images for these nanoparticle arrays shows that the inter-particle spacing measured with GISAXS agrees with the values that can be obtained from TEM images. However, the inter-particle spacing, estimated from the TEM images, for the Small +

Large nanoparticle arrays shows that the Small particles are spaced closer together than the Large particles. The Large particle spacing in TEM matches the GISAXS value for the inter-particle spacing. This suggests that the GISAXS measurements of the inter-particle spacing for the Small + Large nanoparticle arrays are dominated by the structure factor scattering for the Large particles. This further suggests that the Large micelle solutions of PS<sub>16500</sub>-*b*-PAA<sub>4500</sub> and metal loading 5 are stable, because the Large particles maintain their spacing with respect to solution concentration, equilibration time, and solution combination.



**Figure 27 GISAXS intensity plot for the Medium 0.5 wt% (black curve) and Medium 0.2 wt% (gray curve) nanoparticle arrays. The Medium 0.5 wt% solution used to fabricate the nanoparticle array had equilibrated for 6 months prior to the sample being spin cast. The Medium 0.2 wt% solution used to fabricate the nanoparticle array had equilibrated for 7 months prior to the sample being spin cast. The inter-particle for the Medium 0.5 wt% 6 month and Medium 0.2 wt% 7 month nanoparticle arrays are 20 nm and 17 nm, respectively.**

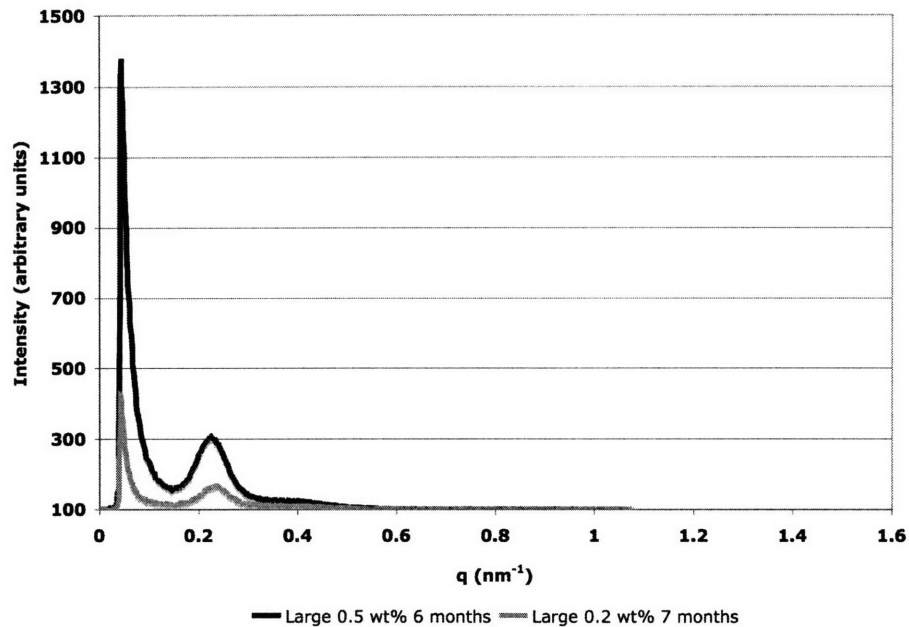


**Figure 28 GISAXS intensity plot for the Large 0.5 wt% (black curve) and Large 0.2 wt% (gray curve) nanoparticle arrays. The Large 0.5 wt% solution used to fabricate the nanoparticle array had equilibrated for 6 months prior to the sample being spin cast. The Large 0.2 wt% solution used to fabricate the nanoparticle array had equilibrated for 7 months prior to the sample being spin cast. The inter-particle for the Large 0.5 wt% 6 month and Large 0.2 wt% 7 month nanoparticle arrays are 28 nm and 27 nm, respectively.**

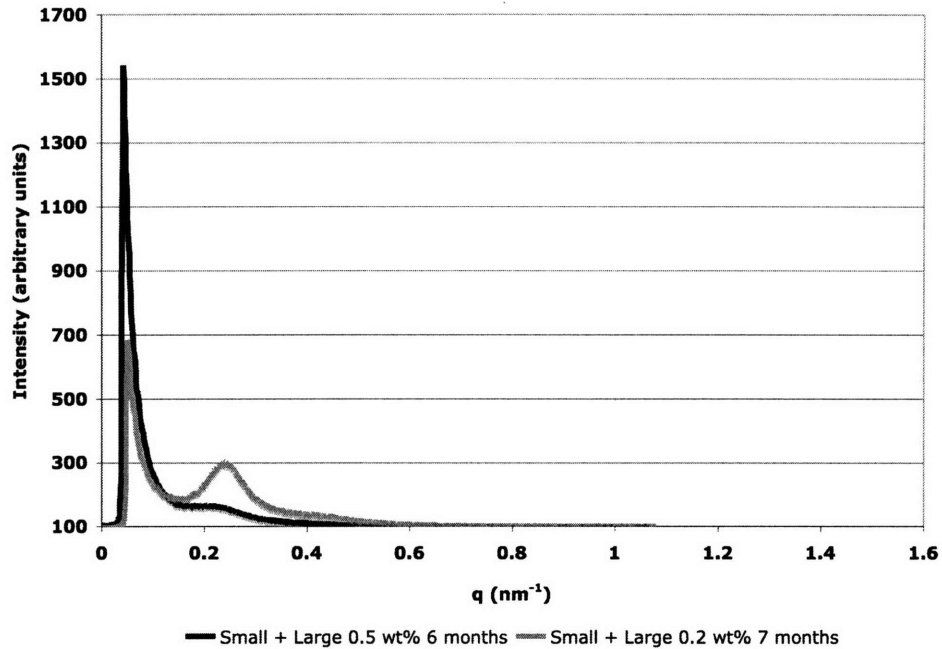


**Figure 29 GISAXS intensity plot for the Small + Large 0.5 wt% (black curve) and Small + Large 0.2 wt% (gray curve) nanoparticle arrays. The Small + Large 0.5 wt% solution used to fabricate the nanoparticle array had equilibrated for 6 months prior to the sample being spin cast. The Small + Large 0.2 wt% solution used to fabricate the nanoparticle array had equilibrated for 7 months prior to the sample being spin cast. The inter-particle for the Small + Large 0.5 wt% 6 month and Small + Large 0.2 wt% 7 month nanoparticle arrays are 28 nm and 26 nm, respectively.**

Table 4 below lists the inter-particle spacing that was measured for the Medium, Large, and Small + Large nanoparticle arrays. The inter-particle spacing values measured are categorized according to the solution concentration, and the equilibration time.

**Table 4** Listed below are the nanoparticle arrays for which there were adequate data to plot intensities. The plotted intensities yielded intensity peaks, due to the structure factor of the nanoparticles, that made it possible to calculate the inter-particle spacing. The solution concentration, equilibrium time, and inter-particle spacing are listed.

Inter-particle Spacing as Measured With GISAXS					
Relative Sizes	Block Copolymers	Metal Loading	Solution Concentration	Equilibrium time	Inter-particle spacing (nm)
Medium	PS <sub>11000</sub> - <i>b</i> -PAA <sub>1200</sub>	5	0.5 wt%	6 months	20
Medium	PS <sub>11000</sub> - <i>b</i> -PAA <sub>1200</sub>	5	0.2 wt%	7 months	17
Large	PS <sub>16500</sub> - <i>b</i> -PAA <sub>4500</sub>	5	0.5 wt%	6 months	28
Large	PS <sub>16500</sub> - <i>b</i> -PAA <sub>4500</sub>	5	0.2 wt%	7 months	27
Small + Large	PS <sub>11000</sub> - <i>b</i> -PAA <sub>1200</sub> PS <sub>16500</sub> - <i>b</i> -PAA <sub>4500</sub>	0.5 5	0.5 wt%	6 months	28
Small + Large	PS <sub>11000</sub> - <i>b</i> -PAA <sub>1200</sub> PS <sub>16500</sub> - <i>b</i> -PAA <sub>4500</sub>	0.5 5	0.2 wt%	7 months	26



## **Appendix C: Carbon Nanotube Diameters Grown From Nanoparticle Arrays That Were Spin Cast From 0.5 wt% Solutions**

Carbon nanotubes were grown, in the manner described in 2.5, from nanoparticle arrays that were spin cast using 0.5 wt% solutions. In 3.9 it was found that carbon nanotubes did not grow well using the nanoparticle arrays that were spin cast using 0.2 wt% solutions. It was hypothesized that the 0.2 wt% solutions produced nanoparticle arrays that did not have a great enough areal density of nanoparticles to catalyze carbon nanotube growth. This most recent series of experiments addresses that issue by using nanoparticle arrays spin cast from higher concentration solutions; thereby producing nanoparticle arrays with greater areal densities. SAXS analysis was carried out on the carbon nanotube forests grown from Small + Large, Small + XLarge, Large, and XLarge nanoparticle arrays. However, only the Small + XLarge and single XLarge nanoparticle arrays grew carbon nanotube forests that could be adequately analyzed with SAXS. These samples produced SAXS intensities that could be analyzed, such that a peak corresponding to the carbon nanotube diameter could be fitted. The carbon nanotube diameters are shown below in Table 5.

**Table 5** The diameters of carbon nanotubes grown from nanoparticle arrays that were spin cast from 0.5 wt% solutions are shown. Only the XLarge and XLarge + Small nanoparticle arrays that grew carbon nanotubes are listed. These carbon nanotube forests produced enough SAXS intensity to be analyzed.

Carbon Nanotube Diameters Measured With SAXS			
Relative Sizes – Sample #	Block Copolymers	Metal Loading	Carbon Nanotube Diameter (nm)
XLarge – 1	PS <sub>2200</sub> - <i>b</i> -PAA <sub>11500</sub>	5	12.3
XLarge – 2	PS <sub>2200</sub> - <i>b</i> -PAA <sub>11500</sub>	5	12.9
XLarge – 3	PS <sub>2200</sub> - <i>b</i> -PAA <sub>11500</sub>	5	9.8
XLarge + Small – 1	PS <sub>2200</sub> - <i>b</i> -PAA <sub>11500</sub>	5	9.8
	PS <sub>11000</sub> - <i>b</i> -PAA <sub>1200</sub>	0.5	
XLarge + Small – 2	PS <sub>2200</sub> - <i>b</i> -PAA <sub>11500</sub>	5	8.8
	PS <sub>11000</sub> - <i>b</i> -PAA <sub>1200</sub>	0.5	
XLarge + Small – 3	PS <sub>2200</sub> - <i>b</i> -PAA <sub>11500</sub>	5	7.4
	PS <sub>11000</sub> - <i>b</i> -PAA <sub>1200</sub>	0.5	

XLarge-1 and XLarge-2 did produce carbon nanotubes with average diameters that had a 1:1 correlation with the average diameters of the XLarge nanoparticle diameters analyzed stastically from TEM images in 3.4.3. Bimodal carbon nanotube diameters were expected from these samples. However, none of the carbon nanotube forests that were of high enough quality to be analyzed with SAXS produced any detectable bimodality with respect to the carbon nanotube diameters. The XLarge + Small carbon nanotube forests were not bimodal, and did not have average diameters close to either the size of the Small nanoparticles, or the size of the XLarge carbon nanotube diameters measured for XLarge-1 and XLarge-2.